Modeling the nonlinear rheological behavior of magnetorheological gel using a computationally efficient model

Guang Zhang[1], Yancheng Li[2,3], Yang Yu[3], Huixing Wang[1], Jiong Wang[1],

Abstract

Magnetorheological (MR) gel is a novel generation of smart MR material, which has the inherent hysteretic properties and strain stiffening behaviors that are dependent on applied excitation, i.e., magnetic field. The main challenge for the application of the MR gel is the accurate reproduction of the above characteristics by a computationally efficient model that can predict the dynamic stress-strain/rate responses. In this work, parametric modeling on the nonlinear rheological behavior of MR gel is conducted. Firstly, a composite MR gel sample was developed by dispersing carbon iron particles into the polyurethane matrix. The dynamic stress-strain/rate responses of the MR gel are obtained using a commercial rheometer with strain-controlled mode under harmonic excitation with frequencies of 0.1Hz, 5Hz and 15Hz and current levels of 1A and 2A at a fixed amplitude of 10%. Following a mini-review on the available mathematical models, the experimental data is utilized to fit into the models to find the best candidate utilizing a genetic algorithm (GA). Then, a statistical analysis is conducted to evaluate model performance. The non-symmetrical Bouc-Wen model outperforms all other models in reproducing the nonlinear behavior of MR gel. Finally, the parameter sensitivity analysis is employed to simplify the non-symmetrical Bouc-Wen model and then the parameter generalization is conducted and verified for the modified non-symmetrical Bouc-Wen model.

Keywords: Magnetorheological gel, Bouc-Wen model, hysteretic properties, strain stiffening behaviors, sensitivity analysis

1. Introduction

As a novel field-responsive smart material, magnetorheological (MR) gel has emerged recently as an alternative candidate to complement MR fluid. Similar as MR fluid, MR gel is composited of soft magnetic particles such as carbonyl iron powders and gel-like matrix, i.e. polyurethane, and have the following rheological behaviors: the instantaneous shift from the original state to solid-like phase within several milliseconds when subjected to the magnetic field, and reversible return to the gel-like state after the magnetic field is removed. Therefore, MR gel is a kind of magnetic field induced smart material with controllable mechanical properties [1-4].

MR gel can overcome the inherent disadvantage attached to MR fluid such as sedimentation and can achieve a higher MR effect than that of MR elastomer [5-8]. These features equip MR gel with great potentials in engineering applications, such as developing damper and vibration absorber. Till now, there are only a few works been done till now on the development of the MR gel devices [9-11] and the majority of the research on the MR gel focused on the preparation and characterization of the material. Zhang et al [12-13] have investigated the dynamic behaviors of MR gel with the various weight fractions of carbonyl-iron-particle using large-amplitude oscillation shear. The results indicate that the onset strain value from the linear region to the nonlinear viscoelastic area

increases along with the weight of carbonyl-iron-particle. Wang et al [14] synthesized polyurethane-based MR gel with the suspension of the dendritic-like Co and CIP and the rheology behaviors of the MR gel were tested and studied. The result shows that both the yield stress and the stability are greatly improved due to the interaction between CIP and dendritic-like Co. Other work can be found at [15-18]. However, the characterization of the MR gel is still limited to understand the effect of various factors, i.e., CIP contents, the shape of the CIP and material matrix, on the material performance using several indices, i.e., viscosity, storage/loss modulus, MR effect. To date, there is no report on the characterization and modeling of the typical hysteresis behavior of MR gel, which is the essential information for the development of the MR gel devices.

The dynamic mechanical properties of the MR gel are expected to be sitting between MR fluid and MR elastomer, which expresses viscous and/or elastic behaviour upon the application of excitation. As expected, the most challenging task with dynamic behaviors of MR materials is to accurately describe the dynamic mechanical response by the computationally efficient model, i.e., model with less parameter. There are generally two kinds of models to describe the dynamic properties of other MR materials and devices, i.e. parametric and nonparametric models, which have been proposed for other MR materials and devices. For the parametric model, viscoelastic-plastic model is proposed by Pang et al [19] to predict the dynamic hysteresis properties of MR damper. Bouc-Wen hysteresis operator was used to describe the inherent hysteresis behaviors of stress-strain relationships found in materials or devices [20]. To describe the dynamic viscoelastic behaviors of MR damper more accurately over a broad range of inputs, i.e. amplitude, frequency and magnetic field, the modified Bouc-Wen model was proposed by Spencer et al [21]. Considering the shear thinning and inertial effect of MR material in the pure shear mode, Jansen et al [22] proposed Bouc-Wen hysteresis model-based dynamic model without spring element. Kwok et al [23] proposed a non-symmetrical Bouc-Wen for MR fluid damper, which considers the influence of non-symmetrical hysteresis of viscoelastic behaviors. Zhou [24] proposed a Dahl model to capture the force-displacement of MR damper under a fluctuating magnetic field. Those models are capable to portrait the nonlinear hysteresis behavior of the MR fluids/dampers, and could be further modified to characterize the hysteresis of MR gel.

In this paper, the rheological properties of the MR gel are tested and modeled. During the measurement, at a fixed shear strain amplitude of 10%, harmonic loadings with various frequencies (0.1Hz, 5Hz and 15Hz) under two different current levels (1A and 2A) are adopted to examine dynamic stress-strain/rate behaviors of MR gel. Selective parametric models [19-24] are introduced to predict the shear-stress/rate hysteresis loop of MR gel and find the best fit. Several criteria are used to compare different models in reproducing the material performance of MR gel. Finally, the local parameter sensitivity analysis is employed to simplify the best parameter model and then the parameter generalization is conducted and verified.

2. Material and experimental test

The basic matrix has significant influence on the nonlinear rheological behavior of MR gel. Polyurethane is a type of polymer, which is synthesized by Toluene diisocyanate (TDI) and polypropylene glycol (PPG) [25]. Two segments with different properties exist in the polyurethane polymer chain, i.e., the hard and the soft segments. The hard segments and the soft segments are composed of TDI and PPG respectively, as shown in Fig.1. The viscosity of the polyurethane is dependent on the molar ratio of the TDI and PPG and the higher the value of TDI/PPG, the higher

the viscosity of polyurethane [26]. In this work, the polyurethane is utilized as a basic carrier of the MR gel due to the viscosity of the polyurethane that can be controlled by adjusting the molar ratio of the reactant in the practical engineering application. The molar ratio of the TDI/PPG is selected as 3:1 and the molar mass of TDI and PPG were 174.15$g.mol^{-1}$and 2000$g.mol^{-1}$. The sample preparation can be found at our previous study [27]. There are four steps in the synthesis of the polyurethane - the first step is the preparation of the dry PPG; the following step is the uniformly mixing of the PPG and TDI using mechanical stirrer and store the mixture at 75℃ for 3.5 hours until the chain extension reaction as shown in Fig.2 in [27]; the third step is the reaction with BDO which last about 1.5 hours; finally, toluene was added into the pre-polymer with the internal temperature was maintained at 70℃.

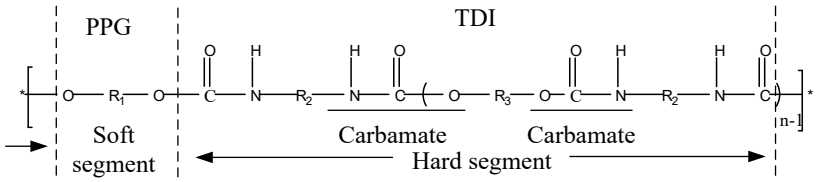

Figure 1. The position of the soft and the hard segment in the chemical units of the polyurethane

Polyurethane based MR gel with 60% of carbonyl iron particles in weight (BASF, Germany, with the diameter ranging from 1 μm to 8 μm and an average diameter of 2.3 μm) is selected as the targeted sample. The MR gel is developed by the following two steps: (1) weighing 120g of carbonyl iron particle and 80g polyurethane matrix respectively by electronic analytical balance (type: CTD-YA522) and slowly pour them into a 250mL beaker; (2) mixing them evenly at an ambitious temperature by using a mechanical stirrer (type: BS-110PRO) and then extract gas using vacuum machine (type: 2XZ-0.5) to obtain MR gel, which is shown in Fig.2(C).

The dispersion of micro-particles in MR gel after curing when no magnetic field applied is observed by a scanning electron microscope (SEM, model: 250FEG), as shown in Fig.2 (A). The gray circle represents particles and the black background is the base matrix. In the sample the larger particles (as highlighted in the red circle) are uniformly dispersed in the polyurethane matrix, and a small part of the smaller powders (as shown in the green circles) are attached to the surface of the larger particles. This is a normal phenomenon due to the obvious van der Waals forces between carbonyl iron particles. Fig. 2 (B) illustrates the chain formation mechanism in the MR gel from off-field to the stages with the magnetic field. From Fig.2 (B), the carbonyl iron particles are uniformly distributed in the matrix at the off- field. After applying a magnetic field, the particles begin to move to form short-chains in the field direction. Further increases the magnetic field, the short-chain becomes longer and thicker. The organized chain structures dismiss immediately to the initial situation after removing the applied magnetic field.

A commercial rheometer (type: MRC302, Anton Paar, Austria) attaching MRD 180 shown in Fig.2(D) is adopted to obtain hysteresis loops of MR gel under harmonic excitation. The appearance of the MR gel at field-off and field-on are shown in Fig 2 (F) as gel-like and solid materials, respectively. To investigate and model the non-linear hysteresis behaviors of MR gel, a large-amplitude-oscillation-stress (LAOS) measurement is conducted to obtain hysteresis responses. Fig.3 shows the hysteresis loops of MR gel excited by harmonic loading of 0.1Hz, 5Hz and 15Hz frequencies at 10% amplitude and three different current levels, i.e. 0A, 1A and 2A.

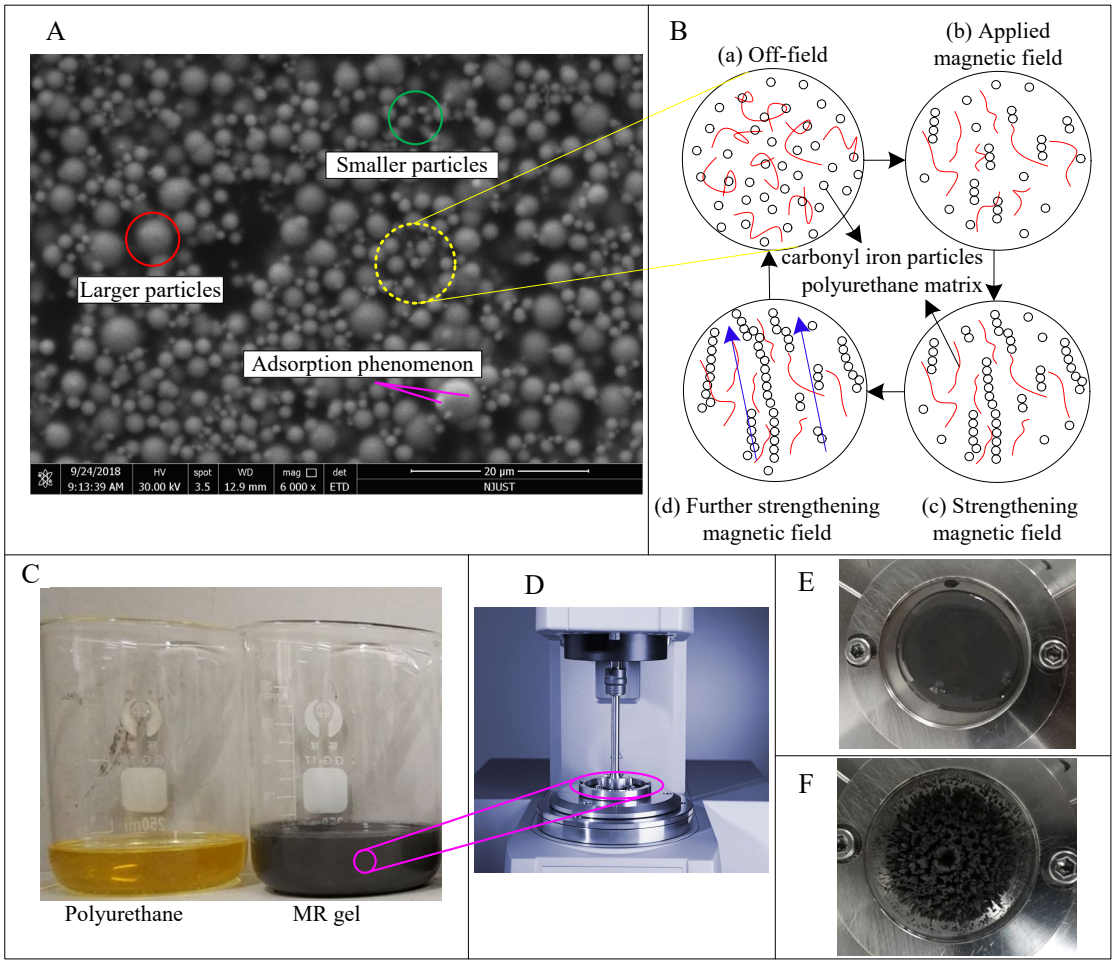

Figure 2. MR gel and experimental setup; (A) microstructure of the MR gel; (B) the response of the MR gel under the application of magnetic field; (C) MR gel and the polyurethane; (D) MCR 302 rheometer; (E) MR gel without magnetic field and (F) MR gel with the magnetic field

The sample exhibits typical viscous properties with the elliptical stress-strain shape when no field is applied. The shear stress-shear rate curves are nearly a straight line in those cases, especially when the excitation frequency is high. Such behaviors are similar to MR fluids since the matrix of the sample is the gel. Increasing the magnetic field, the shear stress-strain hysteresis changes towards typical solid behavior with stiffness emerging with a certain amount of damping. The damping indicates that the MR gel enters the post-yield region. Note that a typical behavior often encountering in MR elastomer appeared for the sample with the applied magnetic field, i.e. strain stiffening [28]. With physical appearance turns to be solid, no surprise that above viscoelastic behavior emerges, which should attribute to the stronger chain structures formed under the influence of the magnetic field. As noted above, the MR gel exhibits complex rheological behaviors with characteristics shifting from fluid to solid. Modeling such nonlinear hysteresis is a necessity to facilitate the understanding of the material behavior and future application of MR gel.

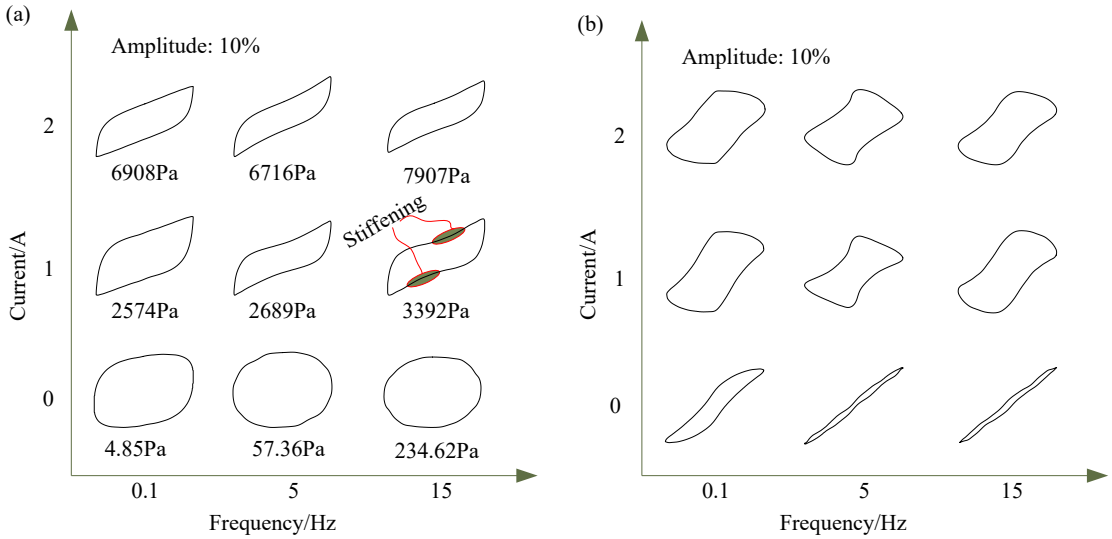

Figure 3. Hysteresis responses of MR gel under sinusoidal excitation; (a) shear stress-shear strain (the number under each loop indicate the maximum stress); (b) shear stress- shear rate

3. Overview of parametric models

3.1 Viscoelastic-plastic model

Considering there are three regions (pre-yield, yield and post-yield stage) during the dynamic process of MR fluid, the viscoelastic-plastic model is proposed in [19, 29]. MR gel has those three regions under the continuous shear similar to MR fluid. The schematic of the viscoelastic-plastic model is shown in Fig.4. It is noteworthy that this model is an extension of the viscoelastic model, in which a yield force is added in parallel with pre-yield and post-yield force. From the Fig.4, the relationship between shear-stress τ and strain x and rate $\dot{x}$ can be described as the following:

$$\tau^{pre} = S_{ve}(\dot{x})\tau_{ve}(x,\dot{x}) + S_{vi}(\dot{x})\tau_{vi}(\dot{x}) + S_y(\dot{x})\sigma_y \quad (1)$$

in which $S_{ve}(\dot{x})$, $S_{vi}(\dot{x})$ and $S_y(\dot{x})$ are shape function given by Eqs (2), (3) and (4), respectively.

$$S_{ve}(\dot{x}) = \frac{1}{2}\left(1 - tanh\left(\frac{|\dot{x}|-\alpha}{4\beta}\right)\right) \quad (2)$$

$$S_{vi}(\dot{x}) = \frac{1}{2}\left(1 + tanh\left(\frac{|\dot{x}|-\alpha}{4\beta}\right)\right) \quad (3)$$

$$S_y(\dot{x}) = \frac{1}{2}tanh\left(\frac{\dot{x}}{4\beta}\right) \quad (4)$$

The viscoelastic properties can be adopted to describe the dynamic mechanism of material internal deformation in the pre-yield region. However, only vicious behaviors can be captured in the post-yield, therefore, $\tau_{ve}(x,\dot{x})$ and $\tau_{vi}(\dot{x})$ in Equ (1) can be expressed as follows:

$$\tau_{ve}(x,\dot{x}) = (k_1 x + c_1\dot{x}) \quad (5)$$

$$\tau_{vi}(\dot{x}) = c_2\dot{x} \quad (6)$$

where k_1, c_1 and c_2 are stiffness and viscous coefficients. There are six parameters should be identified of the viscoelastic-plastic model as shown in the followings:

$$\vartheta = [\alpha, \beta, k_1, c_1, c_2, \sigma_y]$$

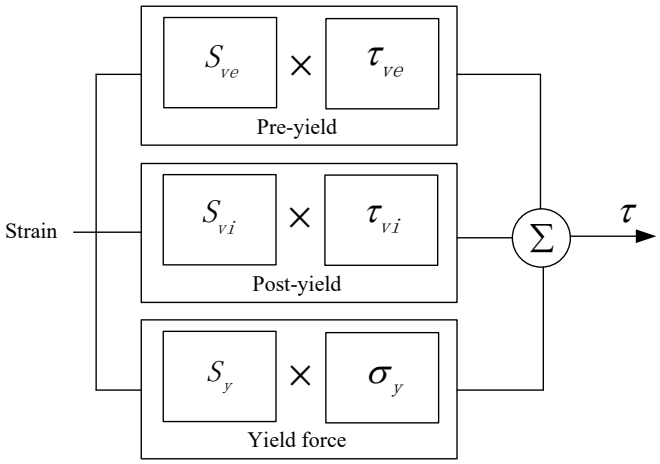

Figure 4. The schematic of viscoelastic-plastic model

3.2 Simple Bouc-Wen model

Simple Bouc-Wen model is proposed to describe the strain stiffening characteristics and highly non-linear relationship between force and displacement [30, 23], shown in Fig.5. The Bouc-Wen is composited of Bouc-Wen hysteresis operator in parallel to a two-parameters viscoelastic model. Therefore, the relationship between stress τ and strain x/rate $\dot{x}$ can be expressed as follows:

$$\tau^{pre} = \alpha z + k_1(x - x_0) + c_1\dot{x} \tag{7}$$

where x and $\dot{x}$ represent shear strain and shear rate of the MR materials respectively; k_1 and c_1 are stiffness and viscous coefficients; x_0 is the initial displacement of spring and z is a Bouc-Wen hysteresis operator, which can be described as following:

$$\dot{z} = A\dot{x} - \beta\dot{x}|z|^n - \gamma|\dot{x}|z|z|^{n-1} \tag{8}$$

where $\dot{z}$ is the time derivative of z; the parameters of A, β and γ control the general shape and scale of the dynamic hysteresis loop and n is used to smooth the hysteresis curve.

To accurately predict the dynamic hysteresis behaviors of MR gel using a simple Bouc-Wen model given by Eqs (7) and (8). A series of eight parameters as shown in the followings should be determined:

$$\vartheta = [A, \beta, \gamma, n, \alpha, k_1, c_1, x_0]$$

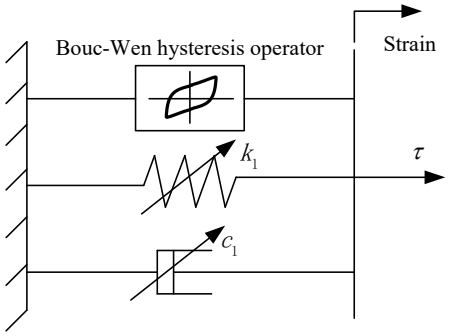

Figure 5. The schematic of simple Bouc-Wen model

3.3 Modified Bouc-Wen model

Considering the incapacity of Bouc-Wen model in predicting the behavior where the velocity and acceleration have opposite signs under the small velocity region, a modified Bouc-Wen model is proposed by Spencer et al [21] to describe hysteresis responses over a broad range of inputs, shown in Fig.6. It is notable that the modified Bouc-Wen is composited of simple Bouc-Wen model in

series with field-dependent dashpot and then in parallel with a field-dependent spring. Therefore, the produced shear-stress τ of the model can be described as follows:

$$\tau^{pre} = c_m\dot{y} + k_m(x - x_0) \text{ or } \tau = \alpha z + k_1(x - y) + c_1(\dot{x} - \dot{y}) + k_m(x - x_0) \quad (9)$$

where x and $\dot{x}$ are the shear-strain and shear-rate respectively; x_0 represent the initial deformation of spring; k_m and k_1 represent the stiffness coefficients of the system and c_1 and c_m are the viscous coefficients of the system; $\dot{y}$ and z represents an intermediate variable and Bouc-Wen hysteresis operator, which can be expressed by the following Eqs, respectively:

$$\dot{y} = \frac{1}{c_m + c_1}(\alpha z + k_1(x - y) + c_1\dot{x}) \quad (10)$$

$$\dot{z} = A(\dot{x} - \dot{y}) - \beta(\dot{x} - \dot{y})|z|^n - \gamma|\dot{x} - \dot{y}|z|z|^{n-1} \quad (11)$$

Where $\dot{y}$ and $\dot{z}$ are the time derivative of y and z, respectively; the parameters of A, β and γ control the general shape and scale of the dynamic hysteresis loop and n is used to smooth the hysteresis curve. Ten model parameters as shown in the followings should be identified:

$$\vartheta = [A, \beta, \gamma, n, \alpha, k_1, c_1, k_m, c_m, x_0]$$

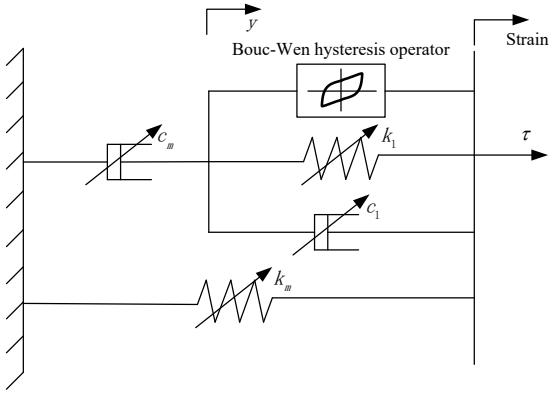

Figure 6. The schematic of the modified Bouc-Wen model

3.4 Bouc-Wen dynamic model without spring element

To capture the shear-thinning effect and inertial effect of MR materials or MR based devices especially in the pure shear mode, a simple Bouc-Wen model without spring element is proposed by Jansen et al [22], shown in Fig.7. Our previous study shows that the developed MR gel has shear-thinning rheological behavior [11,12]. This model consists of a simple Bouc-Wen model in parallel with a dashpot element. Therefore, the shear-stress τ generated by this model can be expressed as following:

$$\tau^{pre} = \alpha z + c_1\dot{x} \quad (12)$$

where $\dot{x}$ is shear-rate; c_1 represents viscous coefficient of the system; z is a Bouc-Wen hysteresis operator, which can be described as following:

$$\dot{z} = A\dot{x} - \beta\dot{x}|z|^n - \gamma|\dot{x}|z|z|^{n-1} \quad (13)$$

where $\dot{z}$ is the time derivative of z; the parameters of A, β and γ control the general shape and scale of the dynamic hysteresis loop and n is used to smooth the hysteresis curve. Six model parameters as shown in the followings should be identified:

$$\vartheta = [A, \beta, \gamma, n, \alpha, c_1]$$

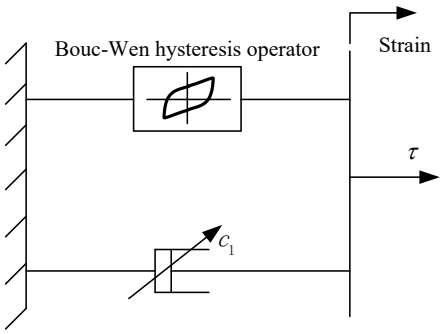

Figure 7. The schematic of Bouc-Wen model without spring

3.5 Non-symmetrical Bouc-Wen model

To describe the non-symmetric hysteresis response accurately, especially in the region of zero velocity, Kwok N et al [23] have proposed a Non-symmetrical Bouc-Wen model, shown in Fig.8. The form of this model is the same as the simple Bouc-Wen, which is composited of non-symmetrical Bouc-Wen hysteresis operator in parallel with a field-dependent two-parameter viscoelastic model. Therefore, the general resist stress of the model can be achieved as follows:

$$\tau^{pre} = \alpha z + k_1 x + c_1 \dot{x} + f_0 \tag{14}$$

where x and $\dot{x}$ represent shear strain and shear rate of the MR materials respectively; k_1 and c_1 are stiffness and viscous coefficients; f_0 is initial stress to offset the hysteresis and z is a non-symmetrical Bouc-Wen hysteresis operator, which can be described as following:

$$\dot{z} = [A - \beta|z|^n - \gamma sgn\{z[\dot{x} - \mu sgn(x)]\}|z|^n][\dot{x} - \mu sgn(x)] \tag{15}$$

where $\dot{z}$ is the time derivative of z; the parameters of A, β and γ control the general shape and scale of the dynamic hysteresis loop and n is used to smooth the hysteresis curve; μ represents the adjust scale coefficient. This model contains nine model parameters to be determined:

$$\vartheta = [A, \beta, \gamma, n, \mu, \alpha, k_1, c_1, f_0]$$

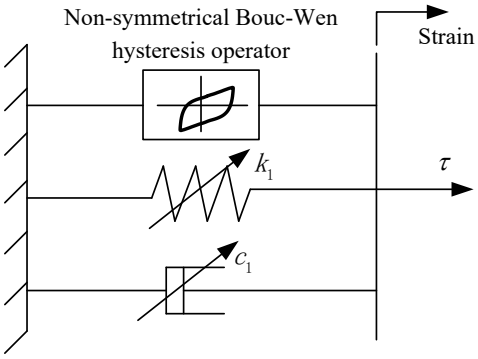

Figure 8. The schematic of non-symmetrical Bouc-Wen model

3.6 Dahl model

Dahl model is proposed by Dahl [31] initially to describe the mechanical system with friction, which models the stress-strain hysteresis response by a differential equation, shown in Fig.9. Dahl model is composited of a Dhal frictional operator in parallel with a field-dependent spring component and a dashpot element. The relationship between output stress and input strain can be expressed as follows:

$$\tau^{pre} = k_1(x - x_0) + c_1 \dot{x} + \alpha z \tag{16}$$

where x and $\dot{x}$ represent shear strain and shear rate of the MR materials respectively; k_1 and c_1

are stiffness and viscous coefficients; x_0 is the initial displacement of spring and z is a Dahl frictional operator, which can be described as following:

$$\dot{z} = \varphi(\dot{x} - |\dot{x}|z) \tag{17}$$

where φ represent stiffness relative parameter in the system. This model has four parameters as shown in the followings to be determined:

$$\vartheta = [\varphi, k_1, c_1, x_0]$$

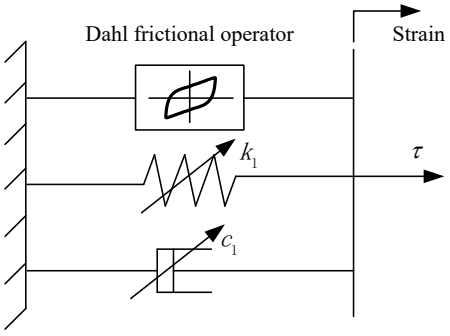

Figure 9. The schematic of Dahl model

4. Problem statement and parameters identified

4.1 Parameter models prediction

After the hysteresis loops have been obtained, the key task is to find the optimal model to capture the shear stress-shear strain and shear stress-shear rate responses of MR gel. Before then, model parameters are to be identified. The schematic of the model parameters identification principle is shown in Fig.10. In this paper, the root mean square error (RMSE) between predict values and experimental values is employed as the fitness function for suitable parameters identification, which is expressed as follow:

$$fit(\vartheta) = \sqrt{\frac{1}{N}\sum_{j=1}^{N}\left(\tau_j^{pre} - \tau_j^{exp}\right)^2} \tag{18}$$

where ϑ represents the model parameters for employed six models described in section 3; N is the number of experimental data in a hysteresis loop; τ_j^{pre} and τ_j^{exp} are the predictive values of employed six models and the experimental values, respectively. The smaller the $\mathrm{Fit}(\vartheta)$ is, the better the parameters are proved. Therefore, the optimal problem can be expressed as the following formulation:

$$\min fit(\vartheta) \tag{19}$$

The model parameters of the above models are solved by the forward Euler method, as follows:

$$z_{j+1} = z_j + \Delta t \cdot \dot{z}_j + o(\Delta t^2) \tag{20}$$

$$y_{j+1} = y_j + \Delta t \cdot \dot{y}_j + o(\Delta t^2) \tag{21}$$

where Δt represents the time interval of experiment sampling.

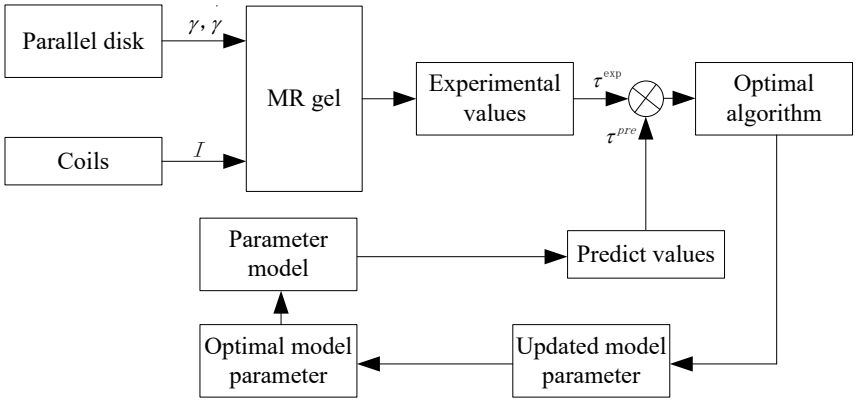

Figure 10. The schematic of model parameters identification principle

In this work, the genetic algorithm (GA) is adopted to solve the optimization problem of parameter identification because of easy coding and fast convergence [32]. MATLAB R2016a is adopted to perform the GA algorithm. The comparison between the model predictions and experimental data are shown in Fig. 11-13. The solid line and point line in those Figs represent prediction values and experimental results, respectively. Tab.2 shows the root mean square error (RMSE) between model description and experimental data, which are obtained by the following expression:

$$\mathrm{RMSE} = \sqrt{\frac{1}{N}\sum_{t=1}^{N}\left(\tau_p - \tau_e\right)^2} \tag{22}$$

where, τ_p and τ_e are predicted stress values and experimental stress values respectively; N is the number of data for one cycle.

It can be observed from Fig. 11-13 that all the parameter models perform good agreement to capture both the stress-strain and stress-rate hysteresis loops of MR gel. Especially, all the parameter models match the experimental results very well under the lower current, i.e., 1A. For the Bouc-Wen model and the Dahl model, both under the current of 1A and 2A, the prediction accuracy reduce along with loading frequency. However, the viscoelastic-plastic model, modified Bouc-Wen model and Bouc-Wen model without spring element can not perfectly portray the test results under the current of 2A and the frequency of 0.1Hz. Among all the employed models, the non-symmetrical Bouc-Wen model can describe the experimental data more perfectly for all test conditions. The main reason for this phenomenon is that the non-symmetrical Bouc-Wen model effectively captures the small asymmetry due to randomly external disturbance during the test. Under the frequency of 15Hz, it appears the unique strain stiffening properties, which can not be captured by the Bouc-Wen model, Bouc-Wen model without spring element and the Dahl model. The about phenomenons can be reflected in Tab.2.

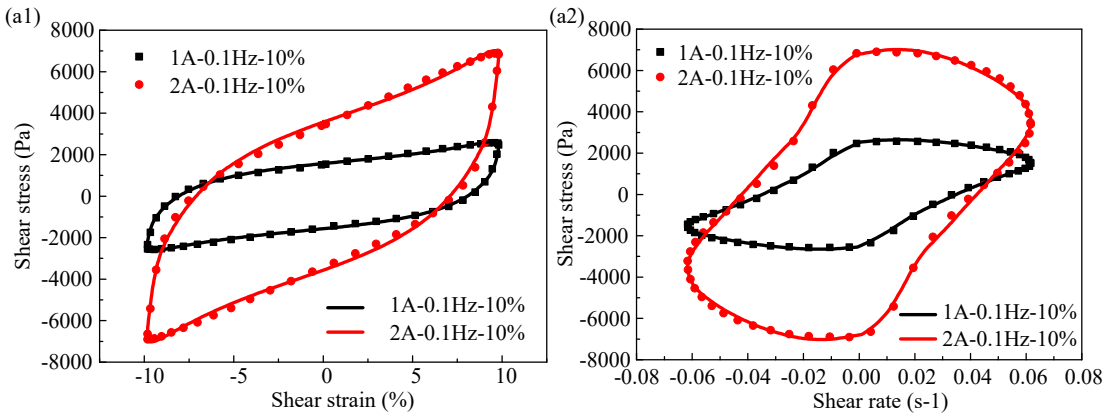

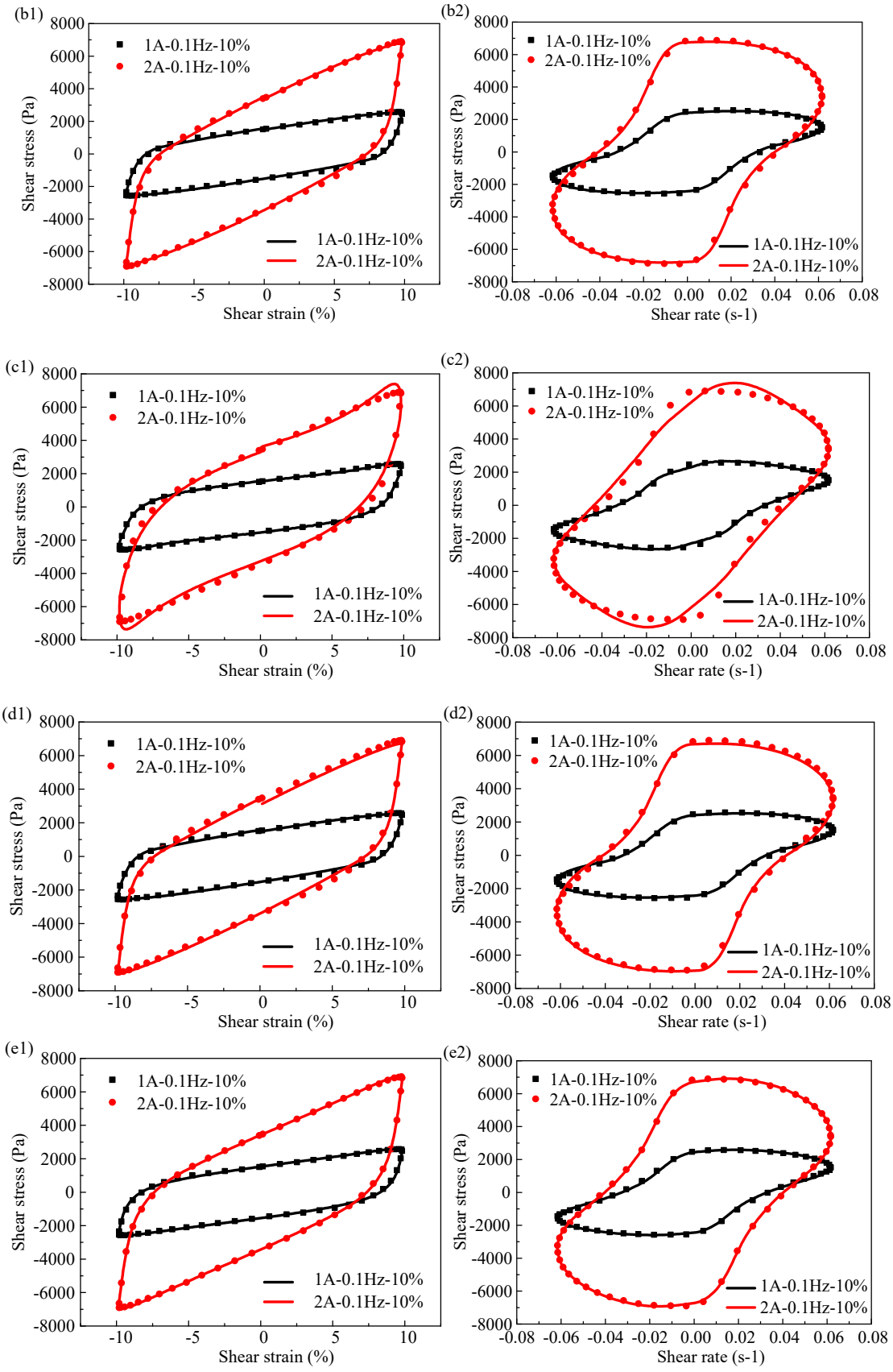
(b1)
(b2)
(c1)
(c2)
(d1)
(d2)
(e1)
(e2)
1A-0.1Hz-10%
2A-0.1Hz-10%
Shear stress (Pa)
Shear strain (%)
Shear rate (s-1)

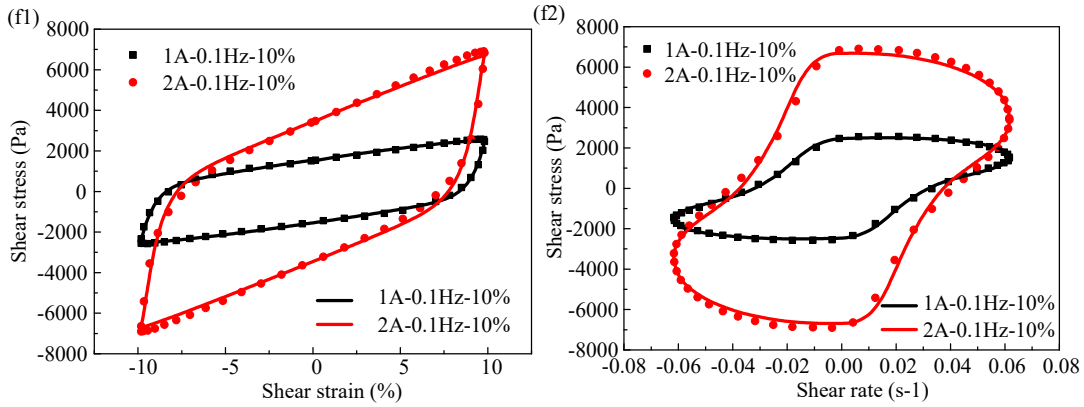

Figure 11. Comparison of stress-strain and stress-rate hysteresis responses between model predictions and experimental measurements under the loading frequency and amplitude are 0.1Hz and 10% at two currents, i.e., 1A and 2A. (a1) and (a2) viscoelastic-plastic model; (b1) and (b2) Bouc-Wen model; (c1) and (c2) modified Bouc-Wen model; (d1) and (d2) Bouc-Wen model without spring element; (e1) and (e2) non-symmetrical Bouc-Wen model; (f1) and (f2) Dahl model.

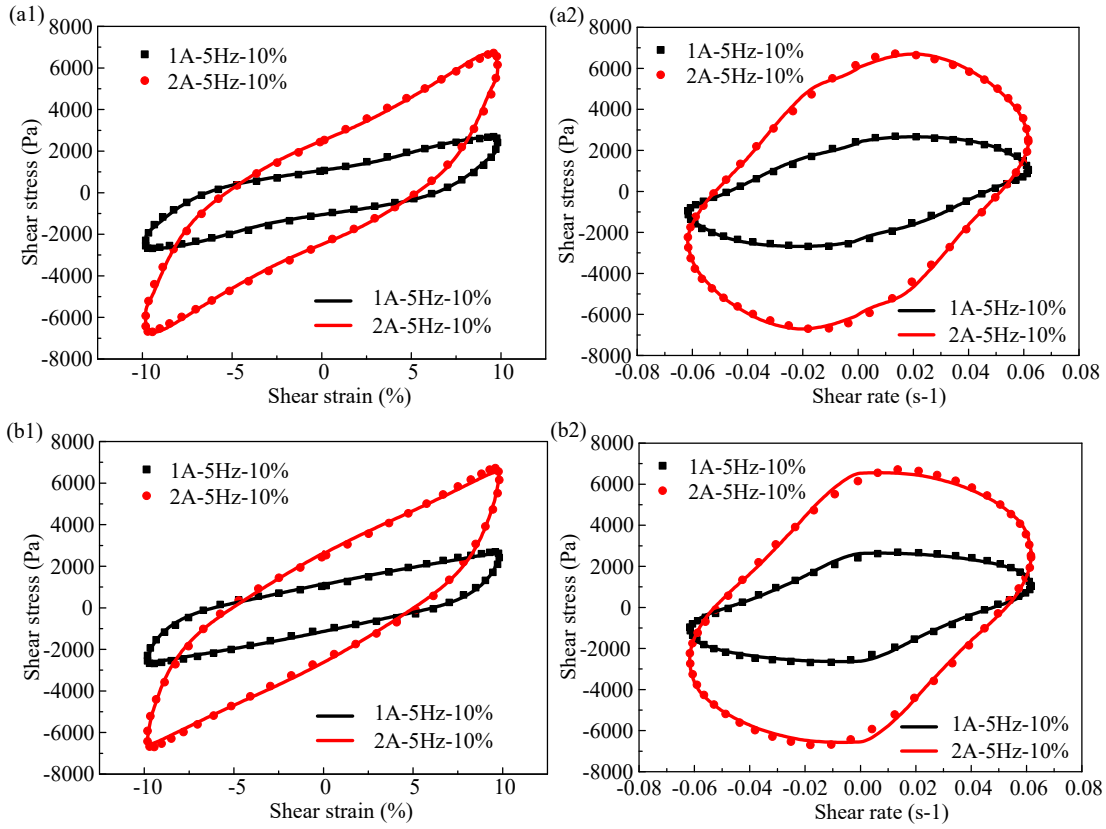

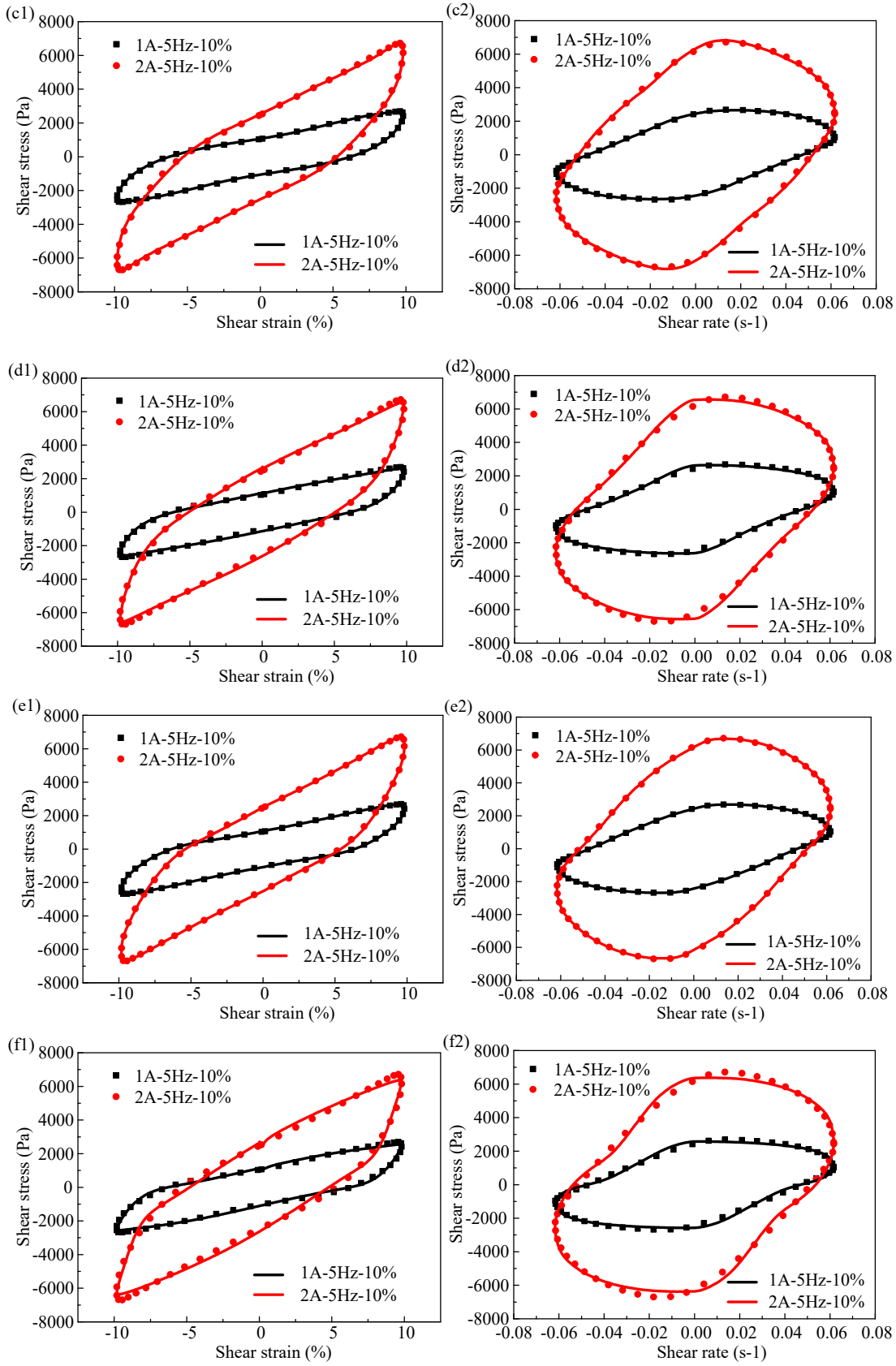

Figure 12. Comparison of stress-strain and stress-rate hysteresis responses between model predictions and experimental measurements under the loading frequency and amplitude are 5Hz and 10% at two currents, i.e., 1A and 2A. (a1) and (a2) viscoelastic-plastic model; (b1) and (b2) Bouc-Wen model; (c1) and (c2) modified Bouc-Wen

model; (d1) and (d2) Bouc-Wen model without spring element ; (e1) and (e2) non-symmetrical Bouc-Wen model; (f1) and (f2) Dahl model.

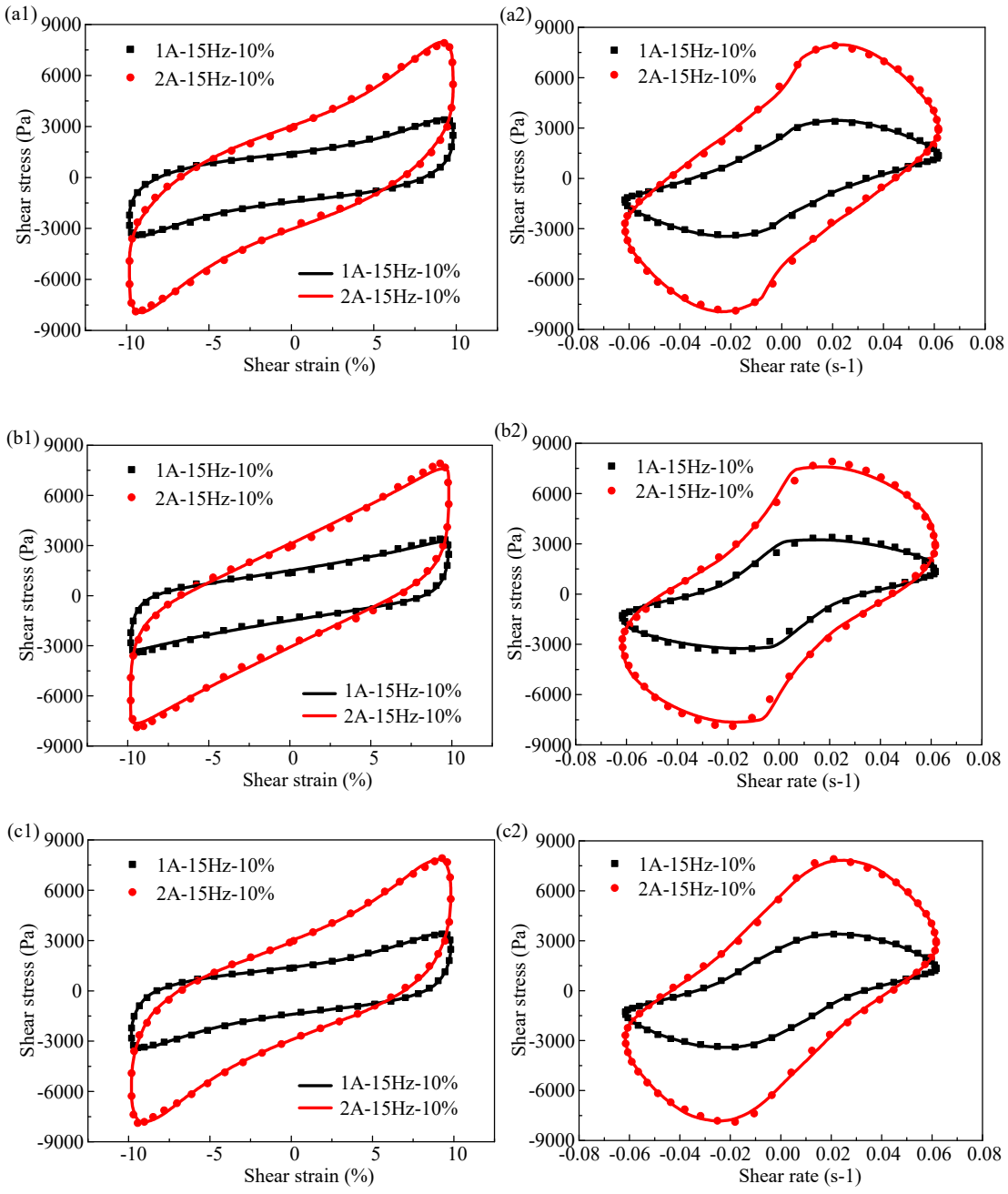

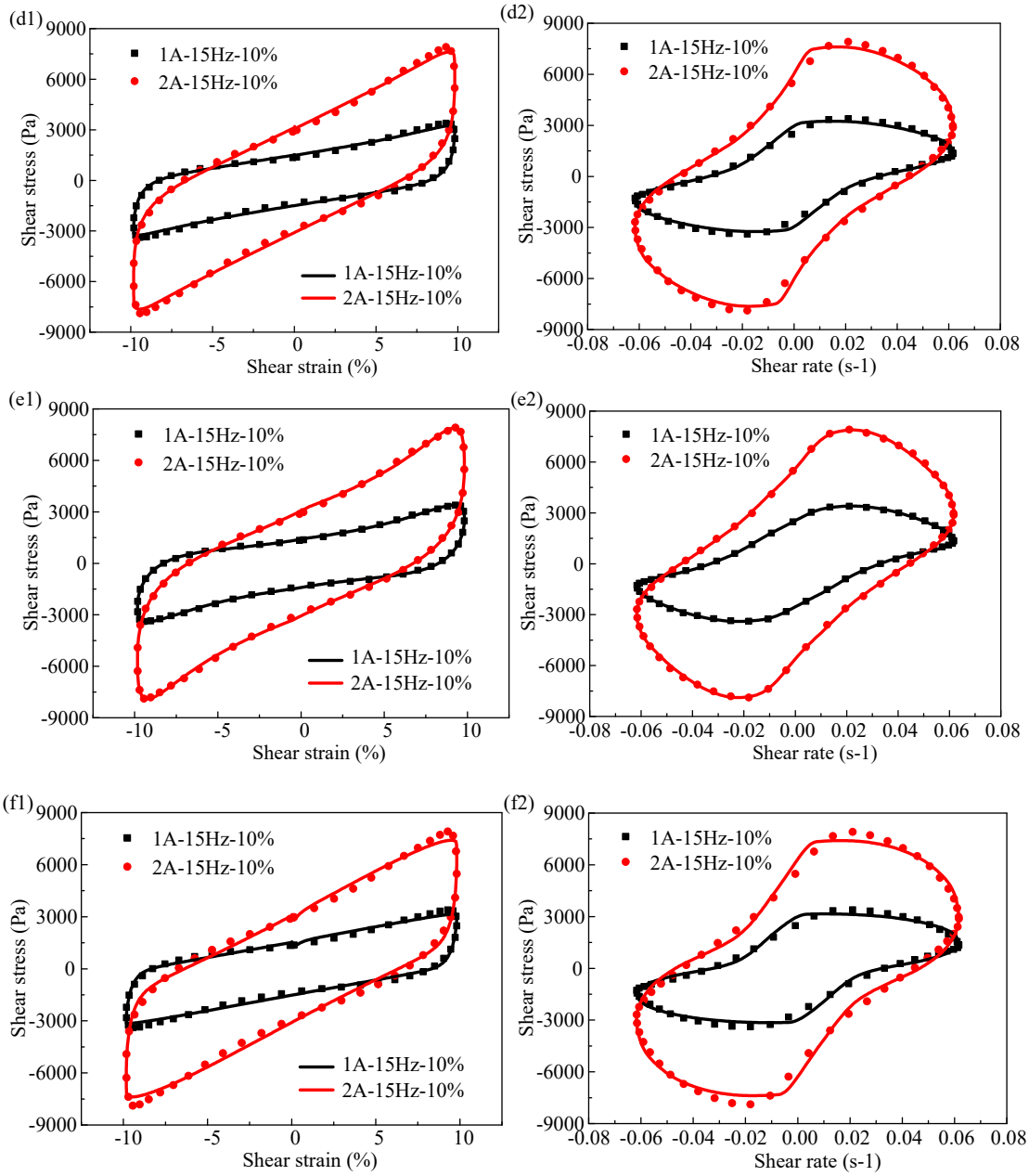

Figure 13. Comparison of stress-strain and stress-rate hysteresis responses between model predictions and experimental measurements under the loading frequency and amplitude are 15Hz and 10% at two currents, i.e., 1A and 2A. (a1) and (a2) viscoelastic-plastic model; (b1) and (b2) Bouc-Wen model; (c1) and (c2) modified Bouc-Wen model; (d1) and (d2) Bouc-Wen model without spring element; (e1) and (e2) non-symmetrical Bouc-Wen model; (f1) and (f2) Dahl model.

Table 2. The RMSE between model prediction values and experimental data under an amplitude of 10%. a. viscoelastic-plastic model; b. Bouc-Wen model; c. modified Bouc-Wen model; d. Bouc-Wen model with mass element; e. non-symmetrical Bouc-Wen model; f. Dahl model.

model	1A-0.1Hz	1A-5Hz	1A-15Hz	2A-0.1Hz	2A-5Hz	2A-15Hz
a	59.61	59.46	65.67	161.49	119.07	136.95
b	74.92	82.27	136.39	117.93	155.30	214.61
c	62.05	24.95	36.49	353.58	88.98	117.60

d	74.09	82.27	136.31	167.99	156.62	213.89
e	51.75	20.58	33.49	54.07	48.03	80.37
f	59.85	108.54	181.02	251.42	238.90	305.97

4.2 Statistical analysis

The RMSE can not characterize the prediction accuracy of the parameter model due to that the greater the loading the higher the shear stress is generated, which leads to the larger RMSE value. Therefore, to further investigate the ability of the model to describe the hysteresis loop of MR gel, the regression analysis method is employed to evaluate the accuracy of the above six models. The determination coefficient k^2 is adopted to appraise the fit confidence of those models, which is described by the following expression:

$$k^2 = 1 - \frac{EXPR}{ENE} \tag{23}$$

$$\mathrm{EXPR} = \sum_{t=1}^{N}\left[\tau_e(t) - \tau_p(t)\right]^2 \tag{24}$$

$$\mathrm{ENE} = \sum_{t=1}^{N}\left[\tau_e(t) - \frac{1}{N}\sum_{m=1}^{N}\tau_e(m)\right]^2 \tag{25}$$

where EXPR is the error square between experimental results and model prediction; ENE represents the total summation of squares. Therefore, the value of k^2 is ranging from 0 to 1. If the value of k^2 is 0, which indicates a complete failure of the model prediction and $k^2 = 1$ indicates a perfect match. Generally, if the value of k^2 is higher than 0.95, it means the parameter model has the capability of capturing the hysteresis responses [33].

Fig.14-19 show the results of regression results of six models for MR gel under all measurement conditions. The slope of the red line is k^2, which is the result of the regression analysis. All the parameter models have the ability to describe the hysteresis behaviors due to the value of k^2 higher than 0.95. Particularly for the non-symmetrical Bouc-Wen model, the value of the regression result is above 0.9990, indicating a high match between experimental results and model prediction, and following by viscoelastic-plastic model.

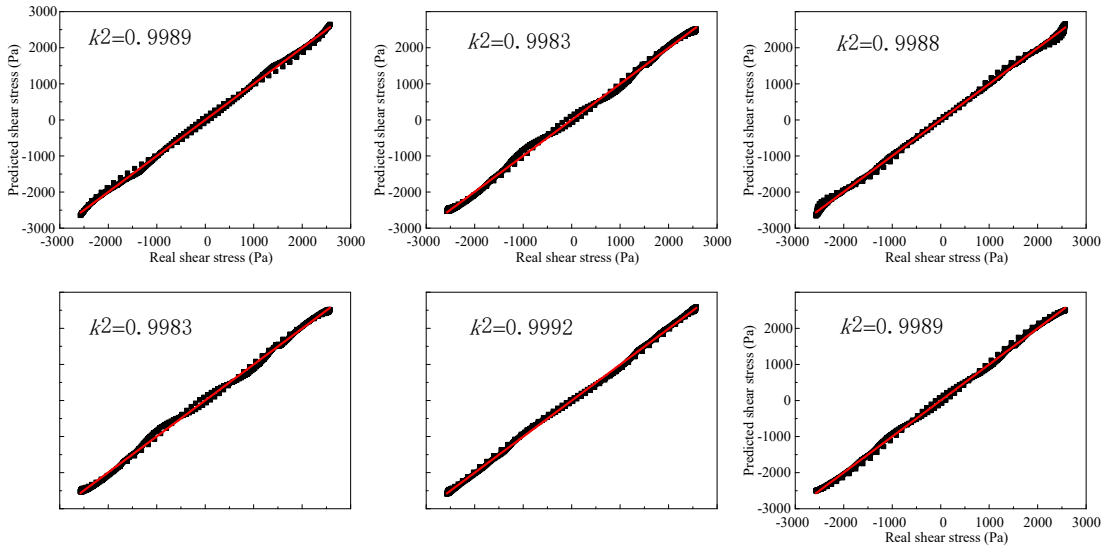

Figure 14. Regression analysis of the parameter models under the loading current and frequency are 1A and 0.1Hz at an amplitude of 10%. (a) viscoelastic-plastic model; (b) Bouc-Wen model; (c) modified Bouc-Wen model; (d)

Bouc-Wen model without spring element; (e) non-symmetrical Bouc-Wen model; (f) Dahl model.

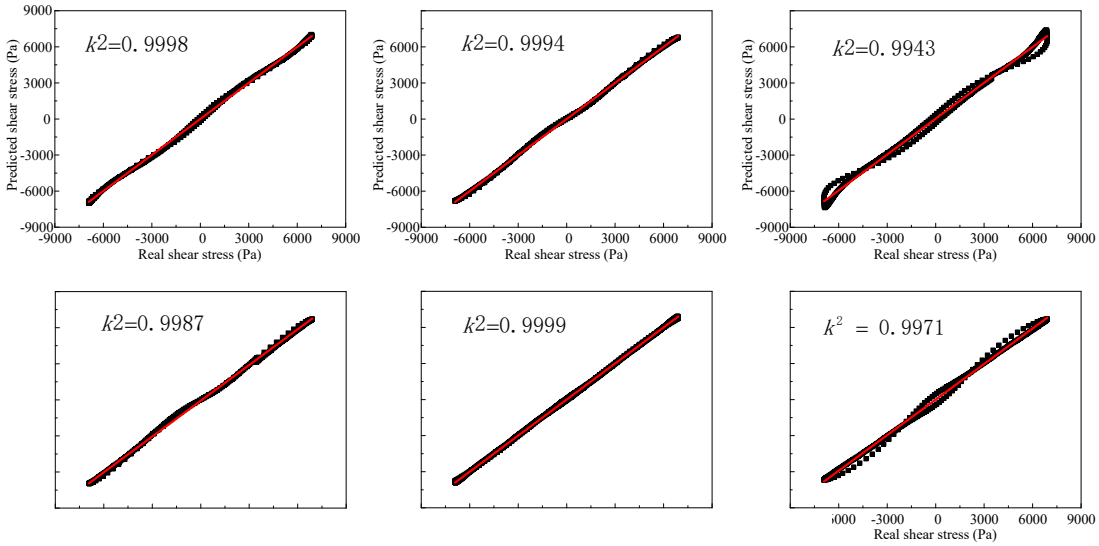

Figure 15. Regression analysis of the parameter models under the loading current and frequency are 1A and 5Hz at an amplitude of 10%. (a) viscoelastic-plastic model; (b) Bouc-Wen model; (c) modified Bouc-Wen model; (d) Bouc-Wen model without spring element; (e) non-symmetrical Bouc-Wen model; (f) Dahl model.

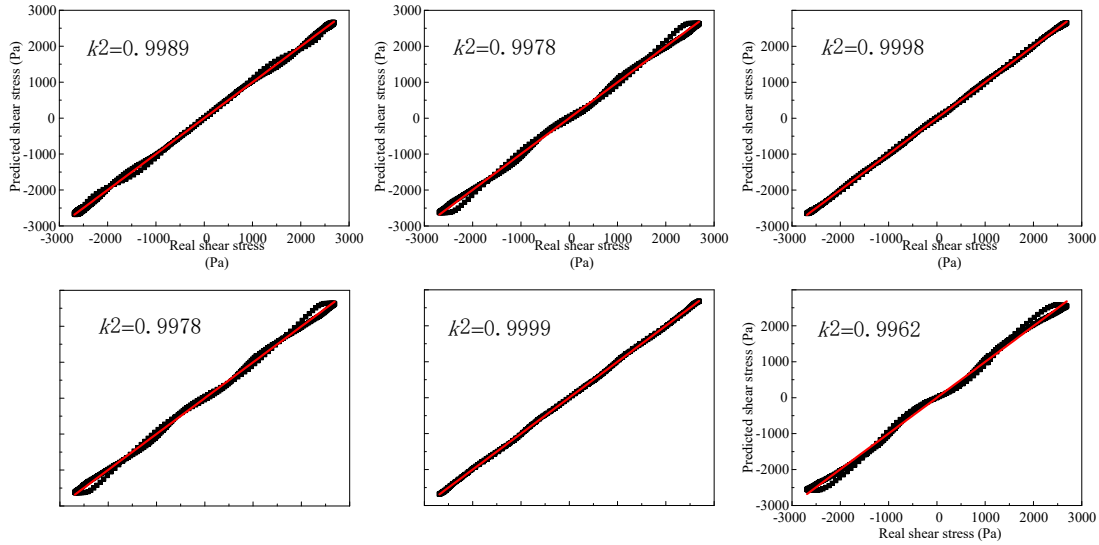

Figure 16. Regression analysis of the parameter models under the loading current and frequency are 1A and 15Hz at an amplitude of 10%. (a) viscoelastic-plastic model; (b) Bouc-Wen model; (c) modified Bouc-Wen model; (d) Bouc-Wen model without spring element; (e) non-symmetrical Bouc-Wen model; (f) Dahl model.

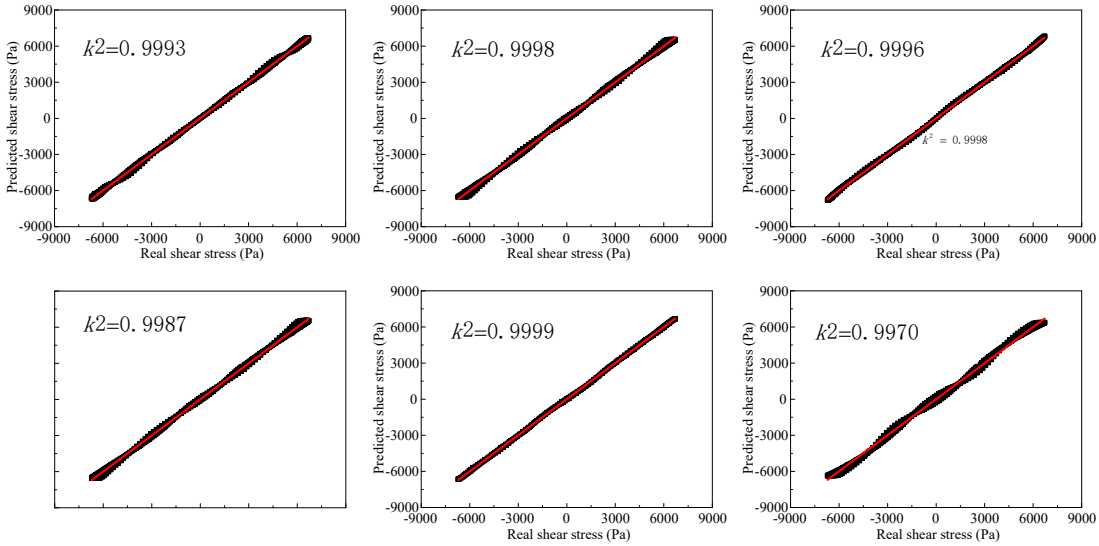

Figure 17. Regression analysis of the parameter models under the loading current and frequency are 2A and 0.1Hz at an amplitude of 10%. (a) viscoelastic-plastic model; (b) Bouc-Wen model; (c) modified Bouc-Wen model; (d) Bouc-Wen model without spring element; (e) non-symmetrical Bouc-Wen model; (f) Dahl model.

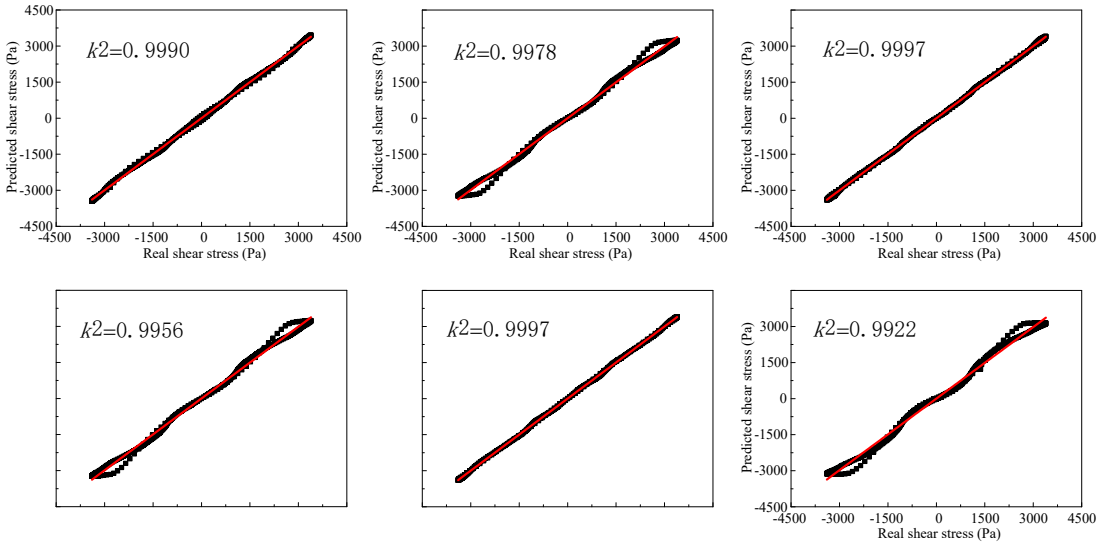

Figure 18. Regression analysis of the parameter models under the loading current and frequency are 2A and 5Hz at an amplitude of 10%. (a) viscoelastic-plastic model; (b) Bouc-Wen model; (c) modified Bouc-Wen model; (d) Bouc-Wen model without spring element; (e) non-symmetrical Bouc-Wen model; (f) Dahl model.

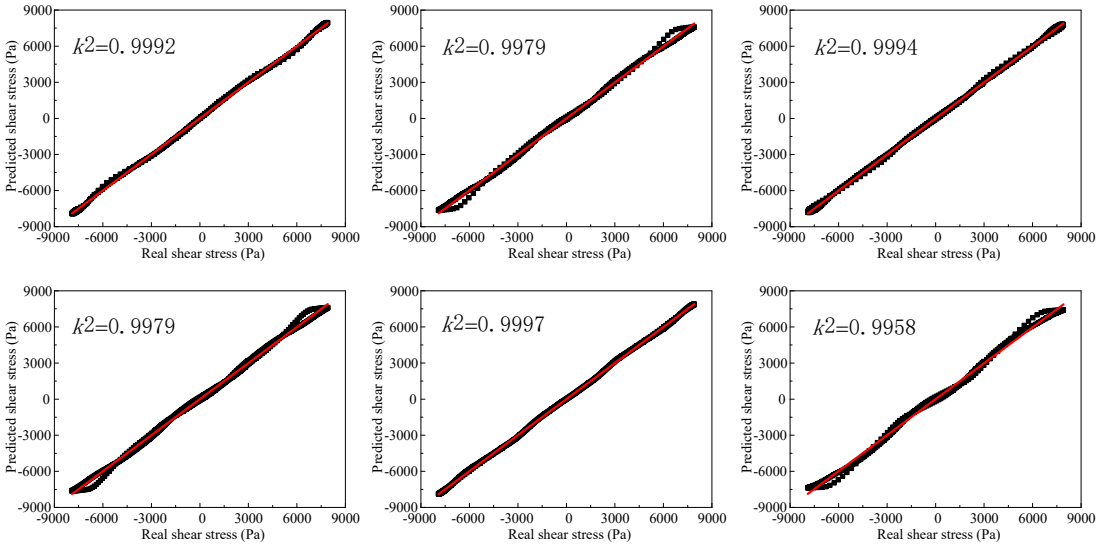

Figure 19. Regression analysis of the parameter models under the loading current and frequency are 2A and 15Hz at an amplitude of 10%. (a) viscoelastic-plastic model; (b) Bouc-Wen model; (c) modified Bouc-Wen model; (d) Bouc-Wen model without spring element; (e) non-symmetrical Bouc-Wen model; (f) Dahl model.

Apart from the RMSE and regression analysis mothed, mean absolute error (MAE) and mean absolute percentage error (MAPE) are employed to comprehensively investigate the ability of mentioned six models in predicting the nonlinear hysteresis of the MR gel. The MAE is defined as the mean absolute error of predicted value relative to experimental value, and the MAPE is defined as the mean absolute error percentage of predicted value relative to the experimental value. The mathematical expression of the MAE and MAPE are expressed in Eqs (26) and (27), respectively:

$$\mathrm{MAE} = \frac{1}{N}\sum_{t=0}^{N}\left|\tau_e(t) - \tau_p(t)\right| \tag{26}$$

$$\mathrm{MAPE} = \frac{1}{N}\sum_{t=0}^{N}\left|\frac{\tau_e(t)-\tau_p(t)}{\tau_e(t)}\right| \times 100\% \tag{27}$$

The statistical analysis of the three evaluation indices, i.e., RMSE, MAPE and MAE, for the prediction performance of the parameter models is conducted, and the results are shown in Fig.20-25. It is indicated that the smaller the three evaluation indices, the better prediction ability the model has. The area surrounded by the red line can reflect the prediction accuracy of the model, and the smaller the area, the more accurate the prediction. Obviously, compared with other parameter models, the non-symmetrical Bouc-Wen model has the minimum area, indicating that the non-symmetrical Bouc-Wen model performs better than other parameter models. Besides, the non-symmetrical Bouc-Wen model has a wider scope of practical application, i.e., from 0.1Hz to 15Hz and from 1A to 2A.

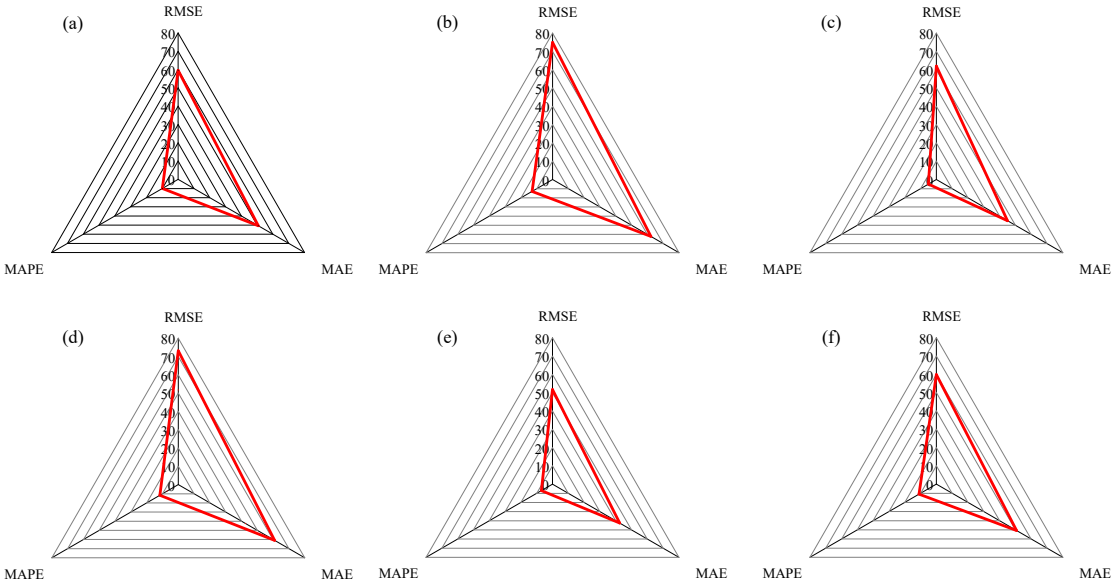

Figure 20. Statistical analysis of the parameter models under the loading current and frequency is 1A and 0.1Hz at an amplitude of 10%. (a) viscoelastic-plastic model; (b) Bouc-Wen model; (c) modified Bouc-Wen model; (d) Bouc-Wen model without spring element; (e) non-symmetrical Bouc-Wen model; (f) Dahl model.

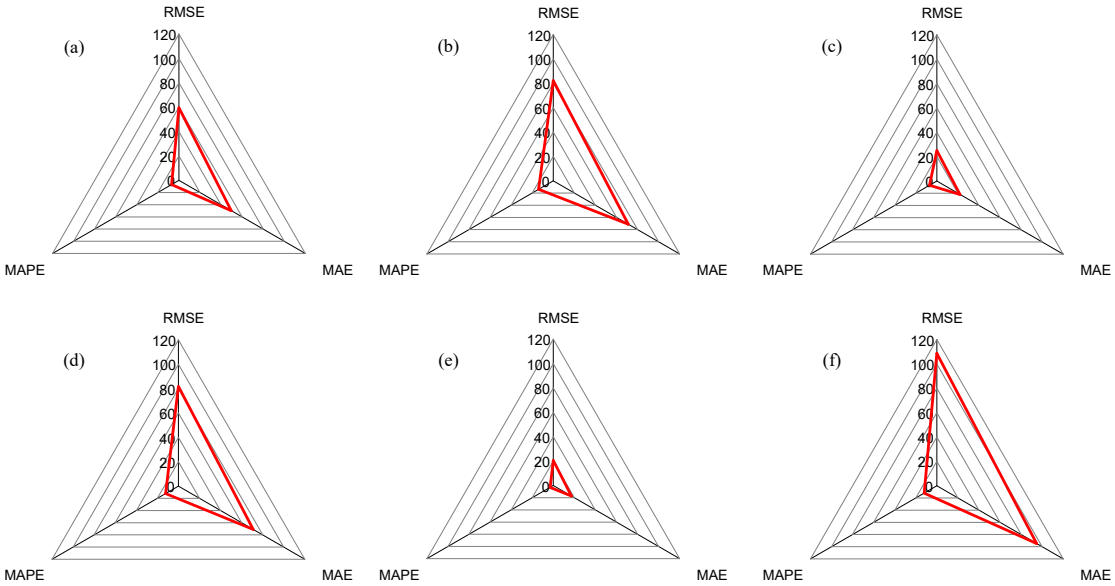

Figure 21. Statistical analysis of the parameter models under the loading current and frequency is 1A and 5 Hz at an amplitude of 10%. (a) viscoelastic-plastic model; (b) Bouc-Wen model; (c) modified Bouc-Wen model; (d) Bouc-Wen model without spring element; (e) non-symmetrical Bouc-Wen model; (f) Dahl model.

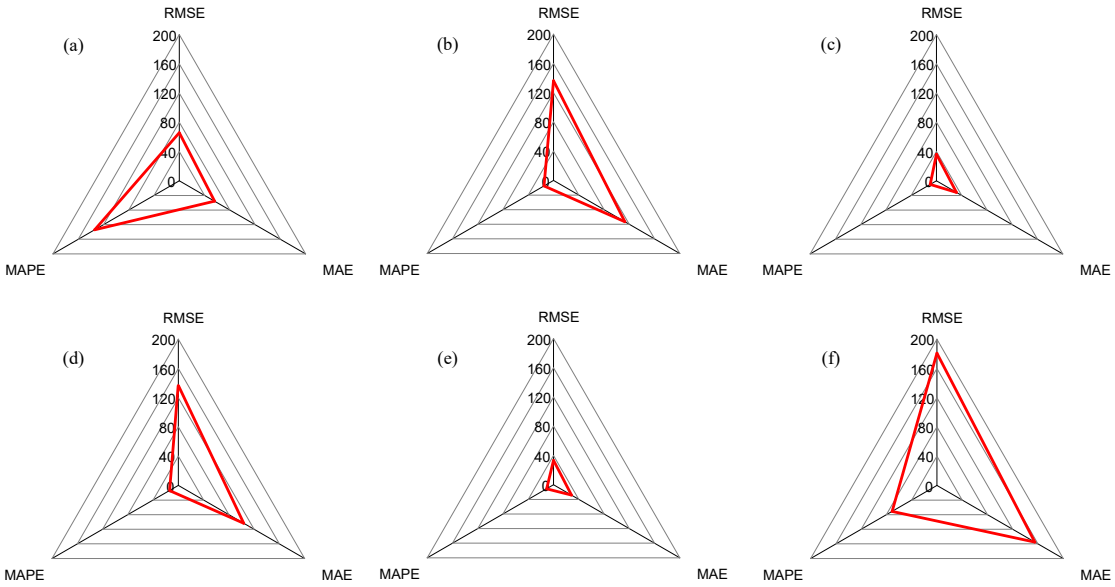

Figure 22. Statistical analysis of the parameter models under the loading current and frequency is 1A and 15Hz at an amplitude of 10%. (a) viscoelastic-plastic model; (b) Bouc-Wen model; (c) modified Bouc-Wen model; (d) Bouc-Wen model without spring element; (e) non-symmetrical Bouc-Wen model; (f) Dahl model.

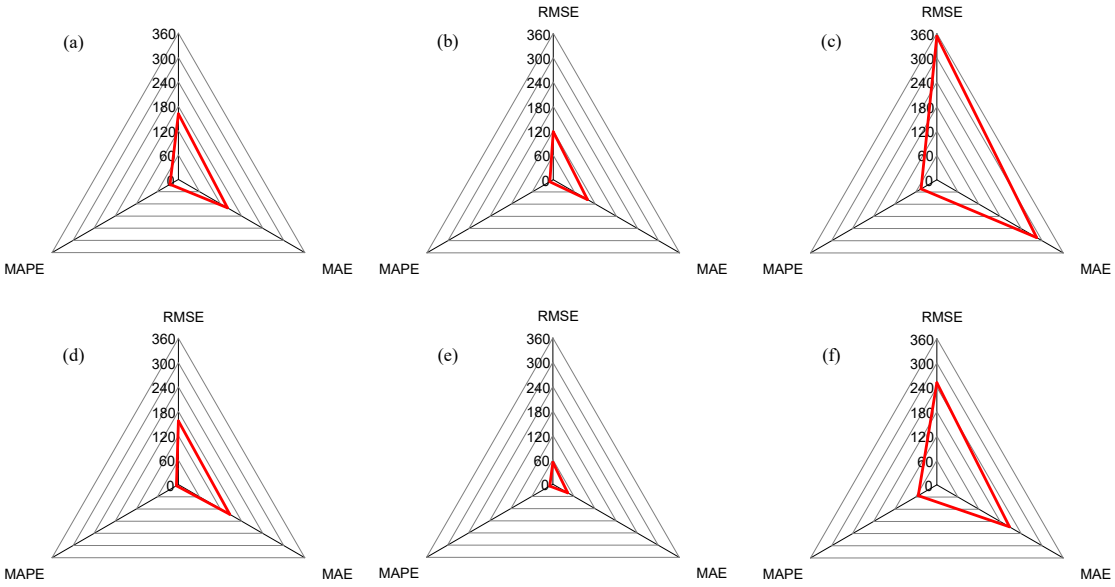

Figure 23. Statistical analysis of the parameter models under the loading current and frequency is 2A and 0.1Hz at an amplitude of 10%. (a) viscoelastic-plastic model; (b) Bouc-Wen model; (c) modified Bouc-Wen model; (d) Bouc-Wen model without spring element; (e) non-symmetrical Bouc-Wen model; (f) Dahl model.

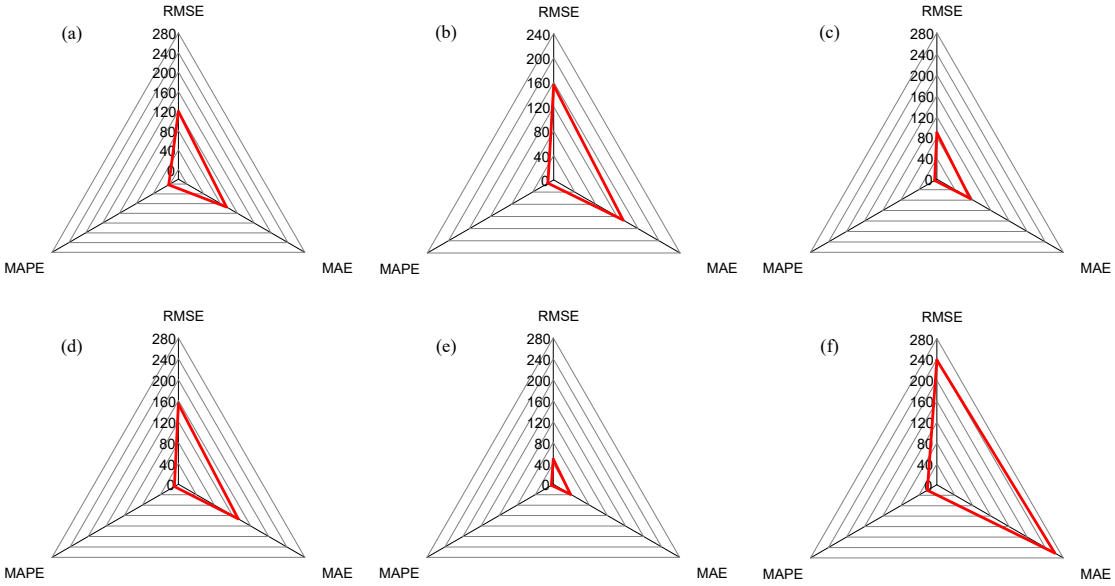

Figure 24. Statistical analysis of the parameter models under the loading current and frequency is 2A and 5Hz at an amplitude of 10%. (a) viscoelastic-plastic model; (b) Bouc-Wen model; (c) modified Bouc-Wen model; (d) Bouc-Wen model without spring element; (e) non-symmetrical Bouc-Wen model; (f) Dahl model.

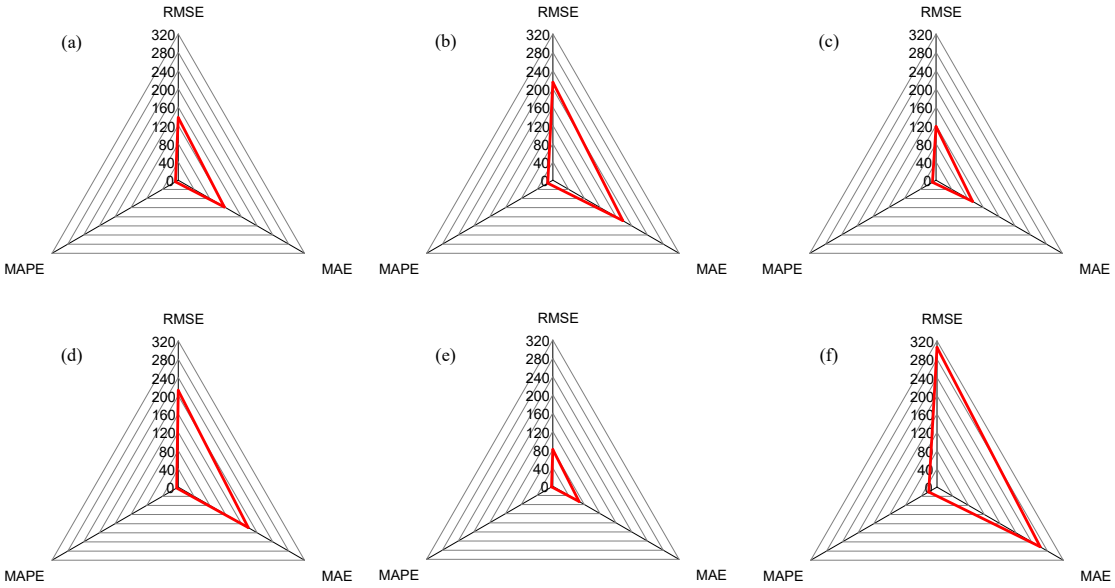

Figure 25. Statistical analysis of the parameter models under the loading current and frequency is 2A and 15Hz at an amplitude of 10%. (a) viscoelastic-plastic model; (b) Bouc-Wen model; (c) modified Bouc-Wen model; (d) Bouc-Wen model without spring element; (e) non-symmetrical Bouc-Wen model; (f) Dahl model.

4.3 Parameter sensitivity analysis

Since the non-symmetrical Bouc-Wen model has the perfect capability to capture the hysteresis properties and strain stiffening behaviors of MR gel compared with other parameter models, the influence of parameter on the model performance needs to be further investigated for the engineering applications. As discussed in section 3 that there are nine parameters of the non-symmetrical Bouc-Wen model, i.e., $\vartheta = [A, \beta, \gamma, n, \mu, \alpha, k_1, c_1, f_0]$. Therefore, to quantitatively investigate the impact of each parameter and obtain a computationally efficient model, parameter

sensitivity analysis is conducted.The local sensitivity analysis method is employed to evaluate the sensitivity of each parameter of the non-symmetrical Bouc-Wen model and its flow chart is described in Fig.26.

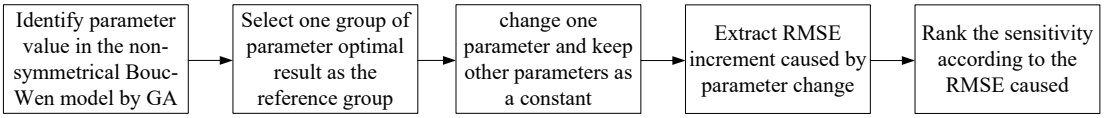

Figure 26. Flow chart of the local sensitivity analysis methods

To make the parameter sensitivity analysis estimation universal, the arbitrary group of the parameter (identified under the current of 1A and the frequency of 5Hz at the amplitude of 10%) of the non-symmetrical Bouc-Wen model is selected as reference values and shown in Tab.3. Every parameter varies from the reference value to $\pm 20\%$ and the generated RMSE between the reference value and change value is employed as the evaluation criterion. Generally, the higher the value of the caused RMSE, the more sensitive it will be. Fig.27 displays the outcomes of parameter sensitivity analysis. It is obvious that k_1 and f_0 are two insensitive parameters in the non-symmetrical Bouc-Wen model and following by μ and c_1. While other parameters belong to sensitive parameters. To give a clear description of the sensitivity of parameters, Tab.4 shows the parameter sensitivity rank for the non-symmetrical Bouc-Wen model.

Table 3. The reference value of the model parameter for sensitivity analysis

Parameter	A	β	γ	μ	α	k_1	c_1	f_0
Value	16.2619	-0.4851	0.2986	0.3295	7.7312	0.5864	146.4187	-0.0475

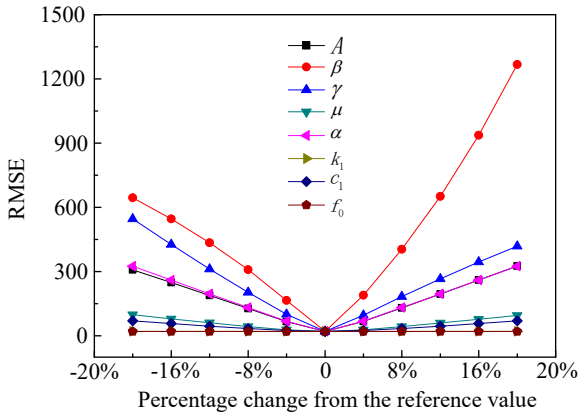

Figure 27. The results of parameter sensitivity analysis of the non-symmetrical Bouc-Wen model

Table 4. The parameter sensitivity rank for the non-symmetrical Bouc-Wen model

Parameter	A	β	γ	μ	α	k_1	c_1	f_0
rank	4	1	2	5	3	8	6	7

Based on the sensitivity analysis, k_1 and f_0 are two most insensitive parameters, which can be set a constant as follows: $k_1 = 0.5864$ and $f_0 = -0.0475$. therefore, the simplified non-symmetrical Bouc-Wen model can be expressed as:

$$\tau^{pre} = \alpha z + 0.5864x + c_1\dot{x} - 0.0475 \quad (14)$$

$$\dot{z} = [A - \beta|z|^n - \gamma sgn\{z[\dot{x} - \mu sgn(x)]\}|z|^n][\dot{x} - \mu sgn(x)] \quad (15)$$

Fig.28 shows the prediction results of the simplified non-symmetrical Bouc-Wen model from the testing data under the frequency of 15Hz and amplitude of 10% with three current levels, i.e., 0A, 1A and 2A. The solid line and point line in Fig.28 represent prediction values and experimental

results, respectively. Tab.5 shows the comparison of root mean square error (RMSE) between the above six parameter models and the simplified non-symmetrical Bouc-Wen model. It is obvious that the simplified non-symmetrical Bouc-Wen model can predict the non-linear hysteresis properties and strain stiffening behaviors perfectly. From Tab.5, the simplified non-symmetrical Bouc-Wen model outperforms Bouc-Wen model, Bouc-Wen model with the mass element and Dahl model because of the lower RMSE value from the testing data under the frequency of 15Hz and amplitude of 10% with currents of 0A, 1A and 2A. Besides, the simplified non-symmetrical Bouc-Wen model shows the best prediction compared with other models at the current of 2A. It means that two parameters are removed from the non-symmetrical Bouc-Wen model, and the simplified one has the great ability to forecast the stiffening properties and non-linear hysteresis behaviors and reduce the computer calculation time meanwhile.

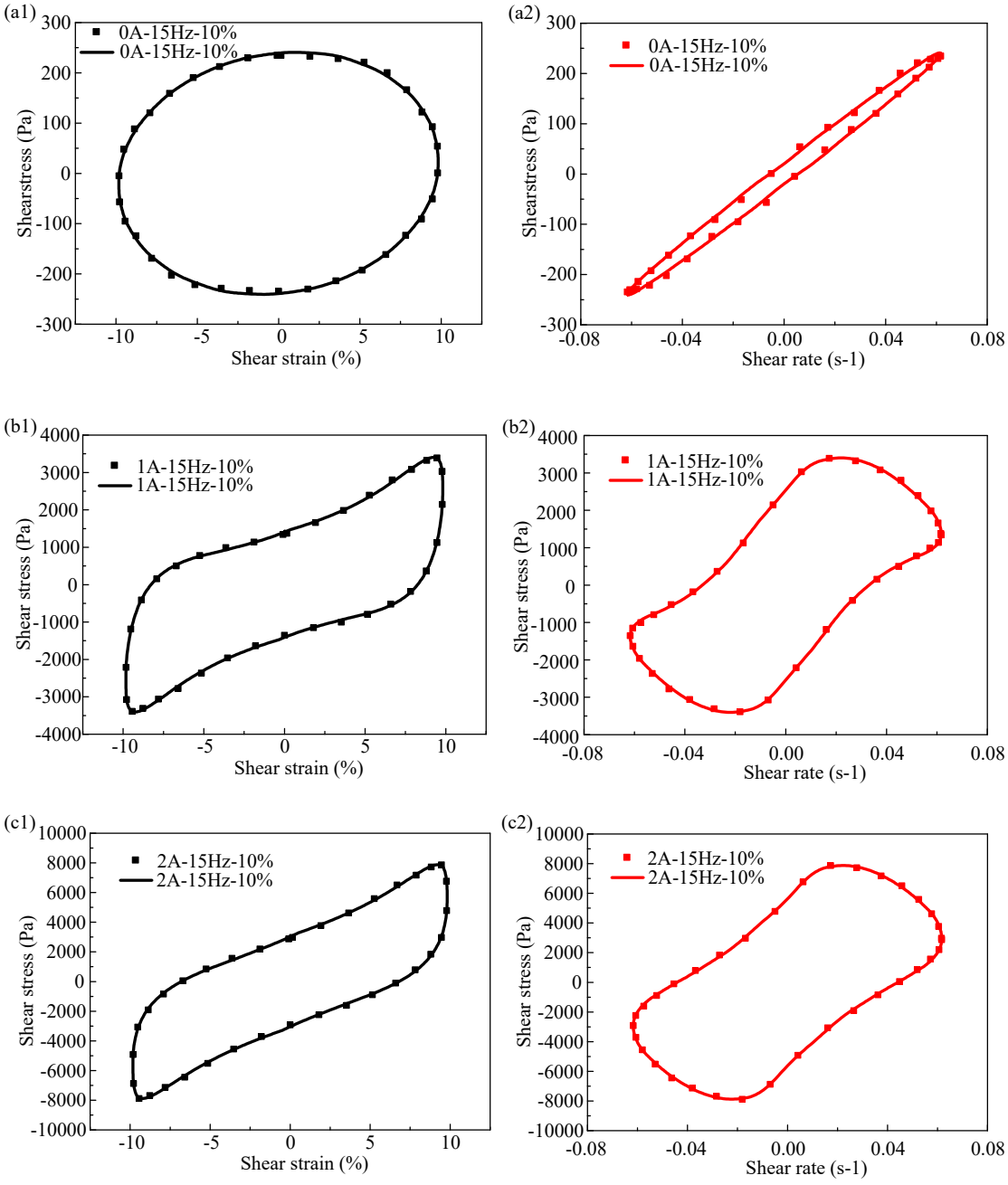

Figure 28. Comparison of and stress-rate hysteresis responses between model predictions and experimental measurements under the loading frequency and amplitude are 15Hz and 10% at three current levels, i.e., 1A, 2A and 3A. (a1), (b1) and (c1) stress-strain loop; (a2), (b2) and (c2) stress-rate loop.

Table 5. The RMSE between model prediction values and experimental data under amplitude of 10%. a. viscoelastic-plastic model; b. Bouc-Wen model; c. modified Bouc-Wen model; d. Bouc-Wen model with mass element; e. non-symmetrical Bouc-Wen model; f. Dahl model; g. simplified non-symmetrical Bouc-Wen model

Model	a	b	c	d	e	f	g
0A-15Hz-10%	4.12	4.72	4.33	3.19	3.65	4.78	3.83
1A-15Hz-10%	65.67	136.39	36.49	136.37	33.49	181.02	80.78
2A-15Hz-10%	136.95	214.61	117.60	214.61	80.37	305.97	76.18

4.4 Parameter generalization

To further study the impact of applied current on the prediction result, the relationship between current and each parameter of the simplified non-symmetrical Bouc-Wen model is also investigated. Tab.6 exhibits each parameter of the simplified non-symmetrical Bouc-Wen model with three current levels, i.e., 0A, 1A and 2A, which is gained by modeling the experimental data corresponding to the frequency of 15Hz and amplitude of 10%. Fig.29 shows the relationship between the applied current and model parameters. The parameter γ monotonically decreases along with the current, while the parameter μ, α and n monotonically increase along with the current at the interval from 0A to 2A. Differently, the parameter A, β and c_1 show a quadratic relationship with applied current. Therefore, the tendency of each parameter with the current can be described by the expressions shown as follows:

$$\mathrm{A} = 22.86465I^2 - 61.95845I + 41.3076 \quad (16)$$

$$\beta = 4.8809I^2 - 14.4451I + 9.3607 \quad (17)$$

$$\gamma = -0.08355I + 0.16865 \quad (18)$$

$$\mu = 65.5059I + 29.8764 \quad (19)$$

$$\alpha = 10.49105I + 0.44518 \quad (20)$$

$$c_1 = -0.98995I^2 + 2.74135I + 0.1544 \quad (21)$$

$$\mathrm{n} = 0.7963I + 0.1073 \quad (22)$$

Table 6. Each parameter values of the simplified non-symmetrical Bouc-Wen model at different current levels, i.e., 0A, 1A and 2A

Parameter	A	β	γ	μ	α	c_1	n
0A-15Hz-10%	41.3076	9.3607	0.1703	25.4222	0.0498	0.1544	0.0375
1A-15Hz-10%	2.2138	-0.2035	0.0818	104.2909	11.7270	1.9058	1.0432
2A-15Hz-10%	8.8493	-0.0059	0.0032	156.4340	21.0319	1.6773	1.6301

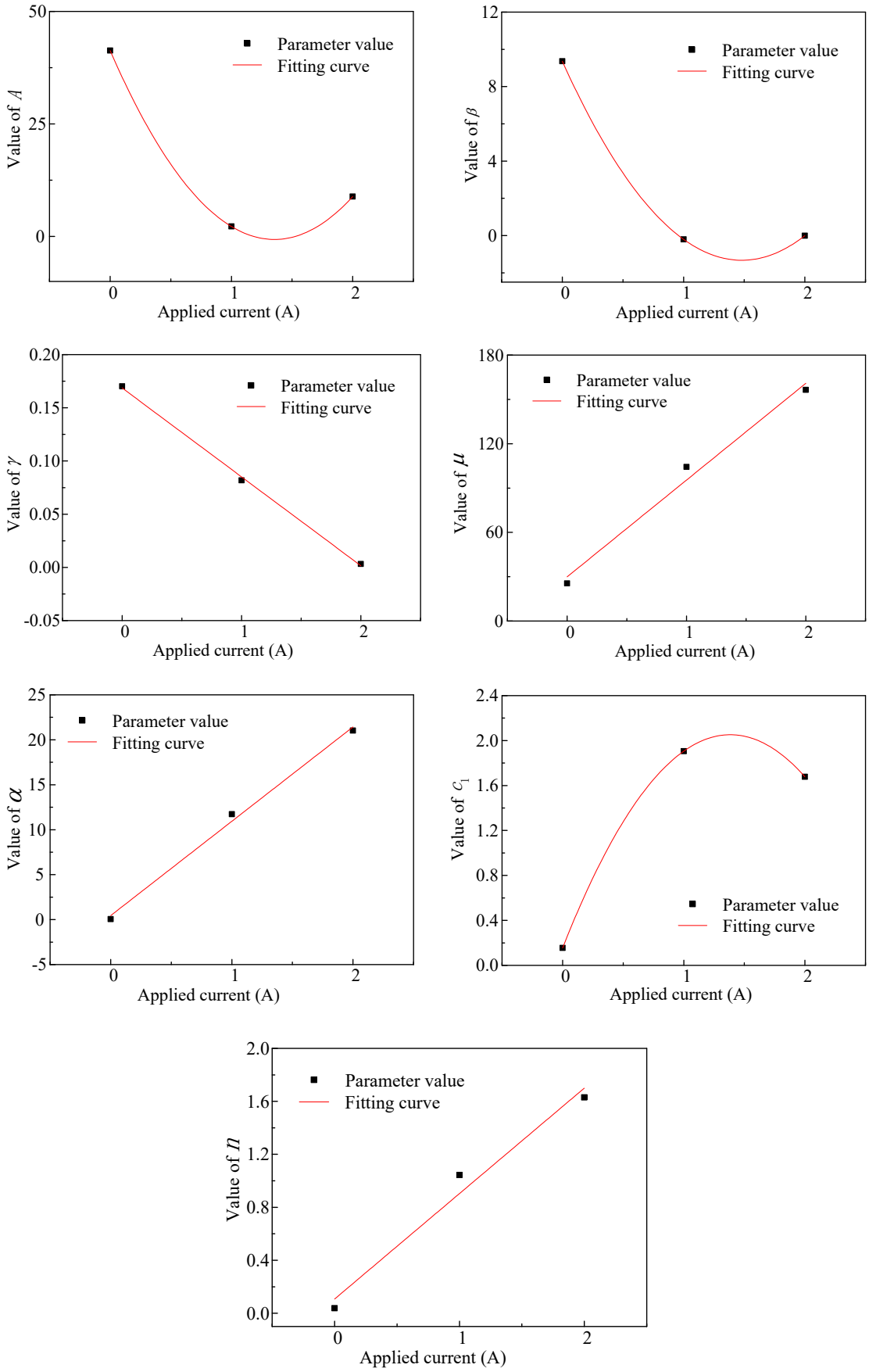

Figure 29. The relationship between the applied currents and each parameter.

Substituting the Eqs16-22 into Eqs14-15, testing data corresponding to the frequency of 15Hz and amplitude of 10% with applied current 0A and 2A is employed to verify the effectiveness of the parameter generalization. Fig.30 shows the comparison between experimental data and prediction curve by the simplified non-symmetrical Bouc-Wen model after parameter generalization. The results indicate that the simplified non-symmetrical Bouc-Wen model with parameter generalization has a great capability to capture the hysteresis and stiffening behaviors of the MR gel. Therefore, this simplified action for the non-symmetrical Bouc-Wen model can bring convenience for modeling the nonlinear hysteresis characteristics of MR gel and further promotes the application of the material in vibration damping.

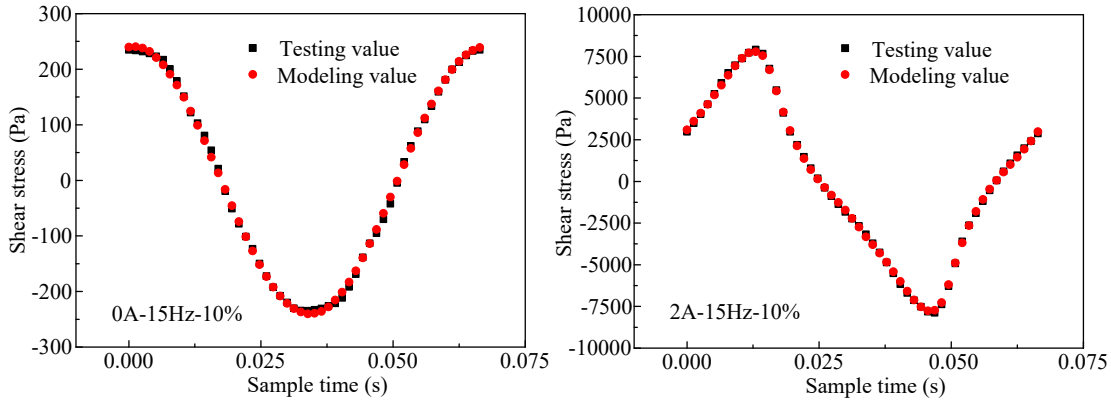

Figure 30. Comparison between experimental data and prediction curve by the simplified non-symmetrical Bouc-Wen model after parameter generalization.

5. Conclusions

This paper explores the establishment of a computational-efficient model for complex rheological behavior of new MR material – MR gel. A polyurethane-based MR gel sample with 60 wt% CIP is characterized using MCR 302 rheometer and it is found that the MR gel collects individually unique characteristics of MR fluid and MR elastomer into one, which brings challenges on the modeling aspect. Searching through the available models for both MR fluid and MR elastomer, a comprehensive modeling process is conducted to locate the optimal model for MR gel. The RMSE between modeling data and testing results is adopted as a fitness function and the GA is utilized to search for the optimal parameters during the identified process. Statistical analysis is conducted to evaluate model performance and the result shows the non-symmetrical Bouc-Wen model stands out from those models. Moreover, the local parameter sensitivity analysis is conducted to reduce the complexity of the non-symmetrical Bouc-Wen model. Finally, a generalization process is introduced to link the model parameters with the input current to reflect the influence of the magnetic field. The result shows that the parameter γ, μ, α and n monotonically changes along with the current, while the parameter A, β and c_1 show a quadratic relationship with the applied current at the interval from 0A to 2A.

Acknowledgments

This work has been supported by a Natural Science Foundation of China (NSFC) grant funded by the Chinese government (No. 51675280, No. 51705467 and 51805209). This work has been also supported by the China Scholarship Council (No.201806840026).

References

[1] Pang H, Pei L, Sun C, et al. Normal stress in magnetorheological polymer gel under large amplitude oscillatory shear[J]. Journal of Rheology, 2018, 62(6): 1409-1418.

[2] Yang P, Yu M, Luo H, et al. Improved rheological properties of dimorphic magnetorheological gels based on flower-like carbonyl iron particles[J]. Applied Surface Science, 2017, 416: 772-780.

[3] An H, Picken S, Mendes E. Direct observation of particle rearrangement during cyclic stress hardening of magnetorheological gels[J]. Soft Matter, 2012, 8(48): 11995-12001.

[4] de Sousa S, dos Santos M, Bombard A. Magnetorheological gel based on mineral oil and polystyrene-b-poly (ethene-co-butadiene)-b-polystyrene[J]. Smart Materials and Structures, 2019, 28(10): 105016.

[5] Xu Y, Gong X, Xuan S. Soft magnetorheological polymer gels with controllable rheological properties[J]. Smart Materials and Structures, 2013, 22(7): 075029.

[6] Wang Y, Wang S, Xu C, et al. Dynamic behavior of magnetically responsive shear-stiffening gel under high strain rate[J]. Composites Science and Technology, 2016, 127: 169-176.

[7] Sharma S, Kumar A. Ride performance of a high speed rail vehicle using controlled semi active suspension system[J]. Smart Materials and Structures, 2017, 26(5): 055026.

[8] Fu J , Bai J , Lai J , et al. Adaptive fuzzy control of a magnetorheological elastomer vibration isolation system with time-varying sinusoidal excitations[J]. Journal of Sound & Vibration, 2019, 456.

[9] Zhang G, Wang H, Ouyang Q, et al. Numerical analysis of multiphysical field for independent three-stage magnetorheological damper of double rod during recoil process of artillery[J]. Proceedings of the Institution of Mechanical Engineers, Part C: Journal of Mechanical Engineering Science, 2019, 233(14): 4960-4979.

[10] Shin B, Yoon J, Kim Y, et al. Note: Vibration suppression using tunable vibration absorber based on stiffness variable magneto-rheological gel[J]. Review of Scientific Instruments, 2015, 86(10): 106106.

[11] Pang H, Xuan S, Sun C, et al. A novel energy absorber based on magnetorheological gel[J]. Smart Materials and Structures, 2017, 26(10): 105017.

[12] Zhang G, Li Y, Wang H, et al. Rheological Properties of Polyurethane-Based Magnetorheological Gels[J]. Frontiers in Materials, 2019, 6, 56.

[13] Zhang G, Wang H, Wang J, et al. The impact of CIP content on the field-dependent dynamic viscoelastic properties of MR gels[J]. Colloids and Surfaces A: Physicochemical and Engineering Aspects, 2019, 580: 123596.

[14] Wang L, Yu M, Fu J, et al. Investigation on the effects of doped dendritic Co particles on rheological property of magnetorheological gel[J]. Smart Materials and Structures, 2018, 27(10): 105041.

[15] Yang P, Yu M, Fu J. Ni-coated multi-walled carbon nanotubes enhanced the magnetorheological performance of magnetorheological gel[J]. Journal of Nanoparticle Research, 2016, 18(3): 61.

[16] Liu B, Du C, Yu G, et al. Shear thickening effect of a multifunctional magnetorheological gel: the influence of cross-linked bonds and solid particles[J]. Smart Materials and Structures, 2019, 29(1): 015004.

[17] Yang P, Yu M, Fu J, et al. Rheological properties of dimorphic magnetorheological gels mixed dendritic carbonyl iron powder[J]. Journal of Intelligent Material Systems and Structures, 2018, 29(1): 12-23.

[18] Kim H K, Kim H S, Kim Y K. Stiffness control of magnetorheological gels for adaptive tunable vibration absorber[J]. Smart Materials and Structures (Print), 2017, 26(1).
[19] Pang L, Kamath G, Wereley N. Analysis and testing of a linear stroke magnetorheological damper[C]//39th AIAA/ASME/ASCE/AHS/ASC Structures, Structural Dynamics, and Materials Conference and Exhibit. 1998: 2040.
[20] Ismail M, Ikhouane F, Rodellar J. The hysteresis Bouc-Wen model, a survey[J]. Archives of Computational Methods in Engineering, 2009, 16(2): 161-188.
[21] Spencer J, Dyke S, Sain M, et al. Phenomenological model for magnetorheological dampers[J]. Journal of engineering mechanics, 1997, 123(3): 230-238.
[22] Jansen L, Dyke S. Semiactive control strategies for MR dampers: comparative study[J]. Journal of engineering mechanics, 2000, 126(8): 795-803.
[23] Kwok N, Ha Q, Nguyen M, et al. Bouc–Wen model parameter identification for a MR fluid damper using computationally efficient GA[J]. ISA transactions, 2007, 46(2): 167-179.
[24] Zhou Q. Two mechanic models for magneto-rheological damper and corresponding test verification[J]. Earthquake Engineering and Engineering Vibration, 2002, 22(4): 144-150.
[25] Xu Y, Gong X, Xuan S, et al. A high-performance magnetorheological material: preparation, characterization and magnetic-mechanic coupling properties[J]. Soft Matter, 2011, 7(11): 5246-5254.
[26] Wei B, Gong X, Jiang W. Influence of polyurethane properties on mechanical performances of magnetorheological elastomers[J]. Journal of applied polymer science, 2010, 116(2): 771-778.
[27] Zhang G, Wang H, Wang J. Development and dynamic performance test of magnetorheological material for recoil of gun[J]. Applied Physics A, 2018, 124(11): 781.
[28] Li Y, Li J, Tian T, et al. A highly adjustable magnetorheological elastomer base isolator for applications of real-time adaptive control[J]. Smart Materials and Structures, 2013, 22(9): 095020.
[29] Kamath G, Wereley N, Jolly M. Characterization of magnetorheological helicopter lag dampers[J]. Journal of the American Helicopter Society, 1999, 44(3): 234-248.
[30] Yang J, Du H, Li W, et al. Experimental study and modeling of a novel magnetorheological elastomer isolator[J]. Smart Materials and Structures, 2013, 22(11): 117001.
[31] Dahl P. Solid friction damping of mechanical vibrations[J]. AIAA journal, 1976, 14(12): 1675-1682.
[32] Yoon Y, Kim Y. An efficient genetic algorithm for maximum coverage deployment in wireless sensor networks[J]. IEEE Transactions on Cybernetics, 2013, 43(5): 1473-1483.
[33] Yu Y, Li J, Li Y, et al. Comparative investigation of phenomenological modeling for hysteresis responses of magnetorheological elastomer devices[J]. International journal of molecular sciences, 2019, 20(13): 3216.